*Manuscript
Click here to view linked References

Retention and enrichment of tungsten-containing carbon films under deuterium beam impact

P.A. Sauter*, M. Balden

Max-Planck-Institut für Plasmaphysik, EURATOM Association, Boltzmannstraße 2, 85748 Garching, Germany

Abstract

Retention and enrichment of a model system for mixed layers, tungsten-containing carbon films (a-C:W), were investigated with respect to the interaction with D ions. a-C:W was exposed to a mass-separated, mono-energetic D beam (200 eV/D, $1.2 \cdot 10^{15}$ D·cm^{-2}·s^{-1}). The W concentration in the films (0-7.5 at%), the specimen temperature during D beam exposure (300 - 1300 K) and the fluence (Φ) of incident D (10^{15} - 10^{20} D·cm^{-2}) were varied. Analysis of retention and enrichment were performed by nuclear reaction analysis and Rutherford backscattering spectrometry, respectively. At 300 K and fluences up to 10^{19} D·cm^{-2}, the increase of the D inventory with fluence in a-C:W cannot be distinguished from a-C and pyrolytic graphite, e.g., above $\sim 10^{17}$ D·cm^{-2} the D inventory increases with fluence according to Φ^x ($x = 0.1$). Above a fluence of 10^{19} D·cm^{-2}, however, the D inventory depends strongly on the W concentration. At a fluence of 10^{20} D·cm^{-2} the D inventory is increased to the 1.5-fold of the D inventory of pyrolytic graphite for 1% and 2.5% a-C:W and it is decreased to the half value of the D inventory of pyrolytic graphite for 7.5% a-C:W. At temperatures above 300 K, following trends are observed: With increasing temperature, the D inventory increases more strongly with fluence and D reaches depths far beyond the width of the ion range. However, the D inventory does not increase with fluence according to Φ^x, especially at fluences above 10^{19} D·cm^{-2}.

PACS: 28.52.Fa, 81.05.U-, 66.30.-h, 79.20.Rf

JNM keywords: Plasma-Materials Interaction, Carbon, Ion Irradiation, Surface Effects, Diffusion

**Corresponding author address:* Boltzmannstr. 2, 85748 Garching, Germany

Corresponding author e-mail: Philipp.Sauter@ipp.mpg.de

Corresponding author phone: +49 89 3299 1923

Corresponding author fax: +49 89 3299 1212

1 Introduction

During the beginning of the ITER operation an enormous entry of energy on plasma facing components is expected, especially at the vertical target, which suggests the use of carbon-fibre-reinforced carbon (CFC) [1] for the hydrogen phase. This choice would result - through the reactivity between deuterium (D) and carbon (C) - in a considerable erosion of C, which would be deposited, during the entire hydrogen phase, in the form of mixed layers on neighbouring areas of the inner vessel wall, together with other sputtered wall materials, e.g., tungsten (W) [2–10].

During the maintenance phase the CFC will be removed by W at the lower vertical target and a couple of recovery techniques will be applied in removing the mixed layers from all areas surrounding the lower vertical target. Nevertheless, the removal efficiency of the recovery techniques is still unclear: No profound experience exists for the application in Tokamks [11]. Furthermore, all previous laboratory experiments point to a rather small efficiency regarding the removal from remote areas and from areas faced to the plasma [12,13]. Therefore, the resolution for the appliance of recovery techniques does not guarantee a sufficient reduction of the mixed layers.

Under the operation with T, mixed layers deposited under a H plasma will act as a reservoir, which could significantly contribute to the build-up of the total T inventory. T can be accumulated in mixed layers by implantation, trapping and diffusion into depth (hydrogen retention). On the other hand, C and T can be accumulated at areas without direct contact to the plasma. The C originates from the re-erosion of the mixed layers from the hydrogen phase. This may lead to an undisturbed formation of T-containing deposited layers during the activated phase,

growing linearly in time [14].

This study is embedded in investigations of the retention and erosion behaviour of deposited layers. The attempt was to investigate the build up of hydrogen inventory in deposited layers through implantation and diffusion into depth. For this purpose, laboratory experiments were performed under defined conditions. At the Garching high current ion source [15] specimens were exposed to a D beam with controlled flux, energy and specimen temperature. This allows characterisation of the retention behaviour under parameter variation.

Besides defined experiments, a material is used, which is similar to deposited layers on one hand and has a defined structure on the other hand. Metal-containing amorphous carbon films (a-C:Me) are a possibility to define a model system for deposited layers [16]. They are produced by dual magnetron sputter deposition with argon working gas. This study is restricted to W-C mixtures, with a concentration of W below 7.5 at%. (Note that this choice was made because of the high erosion of C and the low erosion of W; both are located next to each other at the divertor.) This investigation was carried out by comparing pure carbon films (a-C) and a-C:W. Since a-C and a-C:W have a comparable microstructure [16], it was possible to focus on the influence of the W. Pyrolytic graphite was used as reference material.

In the context of the built-up of tritium inventory in deposited layers, one concern is the accumulation of T through implantation and diffusion into depth. This topic was already investigated for pure graphites, e.g., pyrolytic graphite, and for metal carbide-containing fine grain graphites [17–21] exposed to a D beam. The amount of retained D increased with the amount of incident D, even after saturation of the implantation zone [17–21]. Under a D-T plasma, the T safety limit would be reached after a limited time. In this context, the number of ITER discharges, necessary to reach the safety limit, is determined by the increase of the inventory with fluence. This topic has not been investigated yet for a-C:W. Therefore, the main topic of this study is the D retention behaviour of a-C:W.

The increase of the D inventory with fluence depends on the porosity [20,22]. In fine grain graphites, pore surfaces and grain boundaries act as path ways for diffusion [20]. a-C:W, however, exhibits a kind of porosity, which is not well known yet and which may differ to the porosity of pyrolytic graphite. Another influence is given by the W inclusions. Compared to pyrolytic graphite and to a-C, trapping and diffusion behaviour may be changed intrinsically through the influence of atomically dispersed W inclusions, which change bondings inside the C matrix and in the near vicinity of W inclusions. The evolution of a surface enriched with W through preferential sputtering of C [23], which exhibits an altered reflection coefficient (e.g. for $\geq$12.5% of W in the enrichment zone) and an altered trapping and diffusion behaviour, may lead to a changed D retention behaviour in this shallow zone as well. In this context, the evolution of a W enrichment zone is of major interest, too. The influence of W concentration and of implantation temperature on the enrichment of W has not yet been revealed. In this study results from measurements of the influence of temperature on enrichment are presented and the influence of W concentration on enrichment is discussed taking the erosion yields already published in [24] into account.

In reference [25] the retention behaviour of a-C:W was already characterized and in this study the data base and the interpretation is extended.

After some experimental details in section 2, the influence of implantation temperature on the enrichment of W and on the diffusion of D into depth is reported in section 3.1 and in section 3.2, respectively. In section 3.3 the retention behaviour of a-C:W at 300 K is reported and compared to the retention behaviour of a-C and pyrolytic graphite at 300 K. In section 3.4 the influence of implantation temperature on the increase of the D inventory with fluence in 7.5% a-C:W is presented and the retention behaviour of 7.5% a-C:W at 900 K is compared to the retention behaviour of a-C and pyrolytic graphite at 900 K.

In section 4.1 the influence of implantation temperature on the enrichment of W is discussed for 7.5% a-C:W and the influence of the W concentration is discussed for implantations at 300 K.

In section 4.2 and 4.3 the influence of the enrichment of W and of the diffusion of D into depth is discussed for implantations at 300 K and at elevated temperatures, respectively.

2 Experimental

2.1 Film deposition

Pure carbon films (a-C) and tungsten-containing carbon films (a-C:W) were produced by dual magnetron sputter deposition [26]. A commercial multi magnetron sputter devices was used (Denton Vacuum Discovery 18). Si (100) wafer fragments of 12x15 mm^2 size were used as substrate material, which allows the heat treatment of specimen during D beam exposure. It was shown that the silicon substrate has no influence on the structure of the C matrix and on the W-C-chemistry inside the film for temperatures of 1300 K and below [16]. Before the deposition process, silicon substrates were cleaned in an ultrasonic bath.

For the deposition process W (purity of 99.95%) and graphite (purity of 99.999%) were used as targets. The power at the graphite cathode was supplied by a RF generator (fixed at 500 W). The W concentration was adjusted by selecting a low power between 2 W and 10 W for the DC discharge at the W cathode. Films with W concentrations between 2.5 at% and 7.5 at% were produced. Tungsten concentrations are given in atomic per cent throughout the paper. After four hours of film deposition, a film thickness of $\sim$0.8 -1 μm (obtained from profilometry [16]) was reached, which is the typical thickness of the films investigated.

The areal density of films and the W concentration was determined by Rutherford backscattering spectrometry with ^{4}He at 4 MeV (angle of incidence 0°, scattering angle 165°). The areal densities and the W concentrations obtained at different positions on the specimen were averaged. The averaged values had a standard deviation of 10% and 5%, respectively. The atomic density of the films (unit at/cm^3) was obtained by relating the areal density (unit 10^{18} at/cm^2) to the film thickness. The atomic density for a-C as well as for a-C:W varies between $9 \cdot 10^{22}$ at/cm^3

and $10{\cdot}10^{22}$ at/cm^3, without respect to the W concentration. These values are between the value for a-C:D ($9{\cdot}10^{22}$ at/cm^3) and for the theoretical atomic density of graphite ($11{\cdot}10^{22}$ at/cm^3). The concentration of impurities, such as oxygen, aluminium and argon, was below 2 at%.

As reference material, pyrolytic graphite was used (Grade HPG, Union Carbide; atomic density of $\sim 10.7{\cdot}10^{22}$ at/cm^3). The graphite planes show a mosaic spread of 20° [27]. Plates of 12x15 mm^2 size with 1 mm in thickness were cut with their surface aligned parallel to the graphite planes. The surface was polished with a diamond paste and cleaned in ultrasonic bath.

2.2 Specimen exposure

The D beam is provided by the Garching high current ion source [15]. It produces a D_3^+ ion beam of a flux of $1.2{\cdot}10^{15}$ D/cm^{2}s [25], by extracting and accelerating the D_3^+ ions from the ion source (Oak Ridge type high current injector).

Through the application of a high acceleration voltage, e.g., 3600 V, a high current density is provided. Inside the target chamber the ion beam is decelerated by a positive bias of 3000 V applied at the target. The D_3^+ ion beam is neutralized by an electron cloud at the specimens surface. Thereby, it splits off into three D atoms. For a D_3^+ ion beam accelerated to 3600 eV and decelerated by 3000 V this results in an energy of 200 eV per D atom. Nevertheless, before the D_3^+ ion beam hits the specimen, portions of the beam are neutralized, e.g., at the two apertures in the target chamber. In the incident D beam two particle species simultaneously exist, D_3^+ ions and neutrals (concentration: 10% averaged over the specimen area and about 5% at the reference zone [24,25]). In contrast to the D_3^+ ions, the neutrals are not decelerated by the bias voltage. This leads to an implantation energy of 1200 eV/D for the neutrals. In this context, the term *200 eV D beam exposure* always implicates a coaction of 200 eV and 1200 eV deuterium.

The experimental setup gives the possibility to count the charge accumulated by the D_3^+ ions [15]. From the accumulated charge Q (Cb) the total number of impacting D atoms can be calculated, taking into account that an elementary charge e ($1.6{\cdot}10^{-19}$ Cb) is shared by three D

atoms. By referring the total number of impacting D atoms to an unit area A (cm^2), a fluence Φ (D/cm^2) of incident D can be calculated. The evaluation of the unit area is described in [25], yielding to a value of 0.57 cm^2 for the unit area. This unit area can be identified by an effective area of the erosion spot.

The specimen can be heated by electron bombardment from the rear. The electrons are emitted from a W filament, which is grounded, and accelerated towards the rear side of the specimen, by the positive bias of 3000 V applied at the target. The emission current can be increased up to 25 mA. For a-C and a-C:W deposited on a silicon substrate temperatures up to 1300 K are possible. Before the D beam exposure, the specimens were pre-annealed at $\sim$1300 K for 15 min. During the pre-annealing the temperature of the glowing specimen was measured by a filament pyrometer. During the D beam exposure, the temperature of the specimen was monitored by a infrared pyrometer, which was calibrated during the pre-annealing against the filament pyrometer with an accuracy of $\pm$50 K.

2.3 Characterization technique: Ion beam analysis

After exposing specimens to the D beam, retention and enrichment were analysed by ion beam analysis (IBA). Nuclear reaction analysis (NRA) was performed to obtain the total amount of retained D per unit area (D inventory) and depth profiles of retained D. The depth profiles of W were obtained by applying Rutherford backscattering spectrometry (RBS) under a scattering angle of 165°.

(Note that all IBA data were obtained at the reference zone and related to the fluence of incident D; details of this method are described in [25]. The reference zone yields the respective fluence value with an accuracy of 16%.)

2.3.1 Total amount of retained D

The total amount of retained D per unit area (D inventory) was evaluated by integration of the sharp proton peak in the energy spectrum of protons from the 800 keV D(^{3}He,p)^{4}He nuclear reaction (scattering angle 135°; angle of incidence 0°), using the "Möller-Besenbacher" reaction cross section [28].

To determine the total amount of retained D per unit area, in each analysing experiment a one-dimensional scan was performed by the analysing beam, whereby a series of single values of the total amount of retained D was collected. Single values generated on a part of the scan overlapping with the reference zone were averaged, resulting in an averaged amount of retained D. The averaged amount of retained D a standard derivation and thus a relative error was assigned. The relative error was defined as accuracy. The accuracy of the total amount of retained D per unit area is 10%.

The information depth of this analysing techniques is $\sim$1 μm. Since this value slightly exceeds the thickness of the films and since each D depth profile, obtainded from 7.5% a-C:W exposed to the D beam at 300 - 900 K, shows that more than 95% of the retained D is located within the first 500 nm below the surface (i.e., D does not diffuse into the substrate and the films contain the total D inventory), the detectable amount of retained D does not depend on film thickness.

2.3.2 Analysis of depth profiles of W and D

During the D beam exposure, sputtering processes lead to a loss of C atoms near the surface. With increasing fluence, a subsurface layer enriched with W builds up due to preferential sputtering of C. This layer is denoted as the W enrichment zone. However, after the implantation zone is saturated with D, portions of additional D reach depths beyond the implantation zone. Two depth profiles can be found for a specimen, one for the D content and one for the W content. The depth profile of D is gained from the energy spectrum of the alpha particles originating from the 800 keV D(^{3}He,^{4}He)p nuclear reaction (scattering angle 102°; angle of incidence 0°),

which will be denoted by *NRA spectrum* in the following. The depth profile of W is gained from the energy spectrum of the alpha particles originating from the 1 MeV W(^{4}He,^{4}He)W Rutherford backscattering process (scattering angle 165°; angle of incidence 70°), which will be denoted by *RBS spectrum* in the following. Both energy spectra were converted into depth profiles using SIMNRA software [29].

Depth profiles of W and of D were analysed for the specimens implanted at different temperatures (300 K - 1100 K) and at a fluence of $\sim 10^{20}$ D/cm^2. (Note that only specimens, which were implanted at a fluence of $\sim 10^{20}$ D/cm^2, were analysed, since it was expected that the width of the enrichment zone and the diffusion depth were sufficiently large, after implantations at a fluence of $\sim 10^{20}$ D/cm^2, to give good prospects in avoiding problems with the depth resolution.) Thus, a temperature dependences of the width and the composition of the enrichment zone, and of the diffusion depth and the D concentration was evaluated.

For the depth profiles of W and D, the uncertainty of a depth is given by the depth resolution at depth; the depth, which is just larger than the depth resolution at the surface, is denoted as the *resolvable depth* in the following. The depth resolution, which depends on target composition (i.e. the result of the analysis of the W depth profiles) and experimental setup, can be estimated by using RESOLNRA software [30]. Note that RESOLNRA gives depth resolution and depth in the unit 10^{18} at/cm^2. The unit 10^{18} at/cm^2 was converted into the unit nanometre, by using the literature data of atomic densities given in [31] ($1 \cdot 10^{18}$ at/cm^2 equals 88 nm for C and 158 nm for W; assuming a dense material, i.e., graphite for C and bulk W for W, respectively).

For the evaluation of the depth profiles of W and D surface roughness was taken into account by applying atomic force microscopy (see appendix A). Since the influence of parameters such as W concentration, implantation temperature and fluence on the evolution of surface roughness is not known, it was necessary to figure out, for each specimen, whether it is possible to neglect multiple surface crossings [29] and thus to convert the RBS and the NRA spectrum into a depth profile of W and of D, respectively. Another important aspect of roughness lies in its influence on the depth resolution [29]. A rough surface may be described as a superposition of different

film thicknesses, with a Gaussian thickness distribution corresponding to the full width of half maximum of surface roughness (FWHM of surface roughness) [29]. Some of these thickness values may be lower than the resolvable depth.

2.4 Thermal desorption spectroscopy

For a-C and a-C:W (containing 2.5% and 7.5% of W), which were exposed to the D beam at a fluence of 10^{17} D/cm^2, 10^{19} D/cm^2 and 10^{20} D/cm^2, thermal desorption spectroscopy (TDS) was performed in the experimental device "Thermal Effusion Spectroscopy Setup" (TESS) [32], in order to observe the trapping behaviour of a-C:W and a-C. The remote UHV oven setup was used, and the sample temperature was calibrated as described in [32]. During the acquisition of the TDS spectra, the temperature was ramped up to 1300 K with a temperature ramp rate of 15 K/min. The maximum temperature was held constant for 30 min. The HD signal, the D_2 signal, the CD_4 signal (neglecting small contributions of D_2O to the mass 20 signal) and the signals of heavy hydrocarbons were detected. The D_2 signal and the CD_4 signal were calibrated with a calibration leak. Calibration of the HD signal and the signals of the heavier hydrocarbons was not performed.

3 Results

3.1 Enrichment of W: Depth profiles

Results of investigations on the changes of width and the composition of the W enrichment zone with temperature are presented and discussed in the following. W enrichment is expected to affect the retention behaviour, but is difficult to quantify because of problems with the depth resolution, which will be discussed in the following.

Since the RBS spectra of each 7.5 a-C:W implanted at 300 - 1100 K are not affected by mul-

tiple surface crossings (see appendix A), the RBS spectra were fitted by applying SIMNRA software [29]. The resolvable depth was estimated for each RBS spectrum of the analysed specimens by applying RESOLNRA software [30] for the respective target composition. This value was compared to the width of the W enrichment zone. In performing this comparison it needs to be kept in mind that an uncertainty remains for the width of the W enrichment zone. The sum of the squares of the half of the depth resolution and the half of the FWHM of the surface roughness was defined as measure for the uncertainty of the width of the W enrichment zone. Note, the W concentration slightly influences the resolvable depth. The accuracy of the W concentration is determined by the accuracy of the integration of the W peak in the RBS spectrum. The accuracy of the peak integration is dominated by the accuracy of the charge integration in the RBS experiment, which obtains a value of 5%. However, the influence of the accuracy of the W concentration on the resolvable depth and thus on the accuracy of the width of the W enrichment zone was neglected.

In figure 1, the important length scales for the evolution of the depth profiles are shown. Two horizontal lines indicate the width of the ion range of 200 eV and 1.2 keV D in pure W (6.3 nm and 16 nm, respectively [33]). At 700 K and below, all length scales are close together. The width of the enrichment zone slightly decrease between 300 K (11 nm) and 700 K (8 nm). Taking the error of ± 5 nm into account, it is not possible to decide for any of the data points between 300 K and 700 K whether the width of the W enrichment zone is just resolvable or just unresolvable. Note that at 700 K and below, the width of the error bar (10 nm) matches the difference between the width of the ion range of 200 eV D (6.3 nm) and of 1.2 keV D in pure W (16 nm). Therefore, a range must be given for the width of the W enrichment zone for temperatures at 700 K and below, which is given by the width of the ion range at 1.2 keV as the upper limit and at 200 eV as the lower limit. In order to fit the W peak at 300 K and at 500 K for different widths of the W enrichment zone within this range, the W concentration must obtain values above 90%. The W concentration is very close to 100% and the width of the enrichment zone matches the width of ion range at 300 K and at 500 K so that the W enrichment zone appears to be in steady state at 500 K and below. However, in fitting the W peak at 700 K for different widths of the W

enrichment zone within 6.3 nm - 16 nm, the W concentration must obtain values between 70% and 80%, i.e., around 75%. Above 700 K, the width of the enrichment zone drastically increases with temperature above the width of the ion range at 1.2 keV, above the resolvable depth and above the half value of the FWHM, while the latter value also shows a clear increase with temperature. It is obvious that the width of the W enrichment zone is larger than the resolvable depth at 900 K as well as at 1100 K. The W concentration decreases monotonically to 60% at 900 K and finally to 35% at 1100 K.

3.2 Diffusion of D: Depth profiles

In the subsection 3.2.1 the influence of temperature on the D saturation level inside the implantation zone and on the depth distribution of D is investigated qualitatively. The influence of temperature on the depth distribution of D is quantified in the subsection 3.2.2.

3.2.1 Diffusion and Trapping

The energy spectrum of alpha particles, emerging from the 800 keV D(^{3}He,^{4}He)p nuclear reaction (angle of incidence 0°), is influenced by the depth distribution of D as well as by the correlation effects of surface roughness, e.g., multiple surface crossings [29]. During the D beam exposure, the change in surface roughness with the amount of incident D as well as the depth distribution of D may depend on the specimen temperature. Therefore, a special investigation was performed in order to figure out whether it is, in principle, possible to analyse a depth profile of D, which was obtained from a-C:W implanted with D, by performing NRA. Thereby, the main issue was to figure out whether the shape of the NRA spectrum is dominated by the influence of surface roughness or by the influence of depth profile of D. The solution of this attempt is based on the following method, of which the basic idea is described first and the experimental details are described afterwards:

Within the framework of this investigation, a set of specimens was exposed to the D beam in two

steps. For the first step, fixed parameters (e.g. fluence, temperature) were chosen for each specimen exposed to the D beam, so that each of the specimens would exhibit the same roughness and the same D depth profile just at the beginning of the second step. In the second step, each of the specimens was exposed to the D beam at its own set of parameters (e.g. fluence, temperature). Specifically from the low fluences applied in the second step it was expected to change the D depth profile produced in the first step, without changing the roughness. Note, roughness would lead to a tail towards lower energies in the NRA spectrum [29]. With increasing fluence this tail must change its extent to lower energies, if roughness changed [29]. If roughness remains constant - which was expected - the intensity of the tail must increase in equal portions along the whole energy spectrum [29]. On the other hand, if the D depth profile dominates the shape of the NRA spectrum, the NRA spectrum would be changed in a certain energy range. This energy range represents a depth range, which exhibits a changed D content.

a-C:W, containing 7.5% W, were implanted at a temperature of 900 K and at a fluence of 10^{18} D/cm^2. At this fluence either the heat treatment or the D beam exposure was stopped. If the heat treatment was stopped, D was implanted at additional fluences up to $\sim 10^{17}$ D/cm^2, while the temperature was decreasing exponentially (relaxation time $\sim$90 s). If the D beam exposure was stopped, the heat treatment was continued for different time spans up to 36 s. Alternatively the time span was held constant at 300 s and the temperature was increased once to 1100 K and for another exposure to 1300 K. For a comparison the heat treatment and the D beam exposure were stopped simultaneously.

Figure 2 depicts the NRA spectra of 7.5% a-C:W used for this specific investigation. The intensity of detected alpha particles is plotted over the energy of ejected alpha particles, in a sufficiently large range between 1.75 MeV and 3.25 MeV. For the specimens implanted at 900 K and at a fluence of 10^{18} D/cm^2 a continuum is visible between $\sim$2.0 MeV and $\sim$3.0 MeV. For the specimens implanted at different fluences above 10^{18} D/cm^2 (figure 2 (a)) this continuum is superposed by a peak at high energies, just below 3.0 MeV. The intensity of the peak increases with increasing fluence and decreasing temperature, while the extent of the continuum into depth and

the intensity of the continuum are constant with changing fluence and temperature. This means, the shape of the NRA spectrum changed over a small energy range below 3.0 MeV, of less than 0.25 MeV. As previously mentioned, this kind of change of the NRA spectrum is caused by a changed D depth profile. Changes, which may originate from the influence of surface roughness can be excluded. For the specimens heat treated at 900 K after exposure (figure 2 (b)) the shape of the NRA spectrum did not change with time. Heat treatment above 900 K (figure 2 (c)) led to a decrease of the intensity of the continuum with increasing temperature, not in equal portions along the whole NRA spectrum but pronounced at high energies. The extent of the continuum to lower energies did not change. This kind of change of the NRA spectrum is also expected to be due to a changed D depth profile. Changes, which may originate from the influence of surface roughness can be excluded in this case as well.

The following conclusion can be drawn:

For the specimens in this particular investigation, the NRA spectra were not predominantly influenced by surface roughness. Therefore, the correlation effects of surface roughness, e.g., multiple surface crossings, can be neglected here and thus it is possible to convert these NRA spectra into depth profiles of retained D.

Furthermore, these results lead to the following interpretations:

(1) The peak near the surface ($<$70 nm) in figure 2 (a), which was increasing with decreasing temperature, is caused by an accumulation of D at surface near zones, which can be reached by energetic D. This is interpreted in the following way: Bonding states with a lower binding energy than the thermal energy at 900 K, which were unoccupied before decreasing the temperature, were becoming occupied during the decrease of the temperature; the saturation level of the implantation zone is lowered at 900 K compared to 300 K.

(2) Before the decrease of the temperature, D was able to reach depths ($\leq$600 nm; figure 2 (a)), which are beyond the peak near the surface and thus can not be reached by energetic D.

Consequently, it can be concluded that the tail to lower energies in the NRA spectrum is caused by a diffusive process of D into depth (∼90% of the total inventory), i.e., a-C:W allows a kind of diffusive transport of D into depths beyond the implantation zone. (Note that these depths will be denoted as the *diffusion depth* in the following.)

(3) Bonding states occupied at 900 K during beam exposure are not depleted after the exposure is stopped (figure 2 (b)). This interpretation is confirmed by the release of D towards the surface after the heat treatment at 1300 K (figure 2 (c)). Additional bonding states, which were occupied at 1100 K, were depleted raising the temperature above 1100 K.

(4) Heat treatment at 1100 K and at 1300 K (figure 2 (c)) showed a diffusive transport of D, which is directed towards the surface without the presence of an impacting D beam. In other words, the presence of a D beam is a necessary condition for the diffusive transport of D into depth.

3.2.2 Influence of temperature on the diffusion depth

Analysis of the D depth profiles obtained from 7.5% a-C:W, implanted at 300 - 900 K and at $\sim 10^{20}$ D/cm^2, aimed to quantify the influence of temperature on the diffusion depth.

Figure 3 shows a temperature series of the NRA spectra of 7.5% a-C:W. The intensity of detected alpha particles is plotted over the energy of backscattered alpha particles. The peaks originate from alpha particles from the D(^{3}He,^{4}He)p nuclear reaction at 800 keV [34]. In some cases a pile up (e.g. at 900 K; 0.8 MeV - 2.1 MeV) is present at low energies [34].

Since the NRA spectra of each 7.5 a-C:W implanted at 300 - 900 K are not affected by multiple surface crossings (see appendix A), the NRA spectra were fitted by applying SIMNRA software [29]. Results of the fits, the diffusion depth and the D concentration for each specimen of the temperature series are given in figure 4. The two horizontal, dotted lines mark the range for the width of the implantation zone. At 700 K two data points are given for the diffusion depth and for the D concentration, respectively, one for the surface peak and one for the tail (see inlet in

figure 4 (a)).

At 300 K and at 700 K the peak, which would correspond to the implantation zone, is smeared out to the resolvable depth of 50 nm and 60 nm, respectively. Portions of D, which were transported by diffusive processes from the implantation zone into depths below this range, can not be distinguished from D trapped in the implantation zone. Therefore, high energetic peaks are Gaussian shaped and the D concentrations found by SIMNRA fits (0.05 at 300 K and 0.02 at 700 K) are averaged values over this depth range. The tail at 700 K, on the other hand, is due to a diffusive transport of D into depths beyond the resolvable depth of 60 nm. This can be estimated by looking at the NRA spectrum at 700 K. Alphas with lower energies than the low energy edge of the peak at 700 K ($\sim$2.8 MeV) are originated from depths beyond 60 nm. The tail extends to depths around 0.5 μm. This value is far beyond the resolvable depth and, therefore, slight differences of film thickness caused by surface roughness (FWHM of $\sim$5 nm; see appendix A) can be neglected. 50% of the D inventory are trapped inside the first 60 nm and a portion of 50% is trapped in a further 440 nm. At 900 K the resolvable depth ($\sim$100 nm, due to the low W content in enrichment zone) is larger than the width of the enrichment zone ($\sim$50 nm). Consequently, it is not possible to distinguished between D trapped in the implantation, in the enrichment zone or beyond. Furthermore, it is not possible to distinguish between D trapped below the resolvable depth (100 nm) and D trapped at larger depths, since a wide, homogeneous peak is observed, which points to a rather homogeneous depth distribution of the D concentration. This peak extends to depths of $\sim$0.5 μm, i.e., to the same depth range as already observed at 700 K. The averaged D concentration is 2% and thus larger than the average D concentration of 0.3% in the tail at 700 K. About 80% of the D inventory are trapped beyond the resolvable depth at 900 K.

For the diffusion depths and the averaged D concentrations, of course, uncertainties exist, which rise from the uncertainty of the analysing method. The uncertainty of the D concentration is given by the uncertainty of the integration of the D peak in the NRA spectrum. The uncertainty of the peak integration is dominated by the uncertainty of the differential cross section $d\sigma/d\Omega$ of the 800 keV D(^{3}He,^{4}He)p nuclear reaction, which is not larger than 25%. Estimating accu-

racies for the diffusion depths, surface roughness can be neglected (see appendix A). For each temperature the half value of the FWHM of the surface roughness is small against the diffusion depth (<10%). So these values are not given in figure 4. For the uncertainty of the diffusion depth, the depth resolution at depth can serve as first order approximation.

3.3 Influence of W on D inventory at 300 K

3.3.1 Fluence dependence of the D inventory at 300 K

Figure 5 shows the amount of retained D, n_D, as function of the fluence Φ of incident D in the range between $\sim 10^{16}$ D/cm^2 and $\sim 10^{20}$ D/cm^2, for pyrolytic graphite, a-C and a-C:W with W concentrations of 2.5% and 7.5%, and for an *enriched 7.5% a-C:W* (discussed in subsection 3.3.2). Additionally, a solid line is shown, which has a slope of 100%. Along this line the D inventory equals the fluence of incident D, i.e., 100% of the incoming D are retained. Taking reflection of the incoming D beam into account the gradient of this line is reduced by the value of the reflection coefficient, e.g., 17% for C (dotted line) and 55% for W (dashed line) [35].

Data points obtained for pyrolytic graphite in this study show a fluence dependence, which is determined by processes already observed in graphites and well known in literature [20,36]: Below a fluence of $3 \cdot 10^{16}$ D/cm^2, the data points of pyrolytic graphite are close to the dotted line (17% reflection), taking an accuracy of 10% and 16% for the D inventory and for the fluence, respectively, into account. This means, 100% of the trapped portion of the incoming beam are retained within the width of ion range (the implantation zone). For fluences between $3 \cdot 10^{16}$ D/cm^2 and $1 \cdot 10^{17}$ D/cm^2 data points follow a curve rather than a line through the origin. With increasing fluence the D inventory increases along this curve and the gradient of the curve decreases. This is interpreted as the saturation of the implantation zone at fluences between $3 \cdot 10^{16}$ D/cm^2 and $1 \cdot 10^{17}$ D/cm^2 (saturation level of $3.5 - 4.5 \cdot 10^{16}$ D/cm^2). Above a fluence of $1 \cdot 10^{17}$ D/cm^2, the data points follow a line in a double logarithmic scale and it is possible to fit data points by the power law Φ^X. In this study (200 eV D beam exposure) the magnitude

X obtains the value 0.10 ± 0.02. This kind of increase of the D inventory is interpreted to be driven by a diffusive process of D into depth (a diffusive transport of D into depth), which is retarded by bonding processes between D and C [20,36]. (Note that this diffusive process of D into depth will be denoted as the *diffusion of D into depth* in the following.)

Below a fluence of $4 \cdot 10^{16}$ D/cm^2, the D inventory of a-C and a-C:W can not be distinguished from the D inventory of pyrolytic graphite, within the accuracies mentioned. Therefore, a-C:W does not exhibit an intrinsically changed reflection coefficient compared to pyrolytic graphite (17%) for W concentrations of 7.5% and below.

At a fluence of 10^{17} D/cm^2 the D inventory in a-C is not different compared to the pyrolytic graphite, but the D inventory in a-C:W is slightly lower than in pyrolytic graphite. For instance, in 7.5% a-C:W the D inventory is lowered by about $1 \cdot 10^{16}$ D/cm^2 compared to the D inventory in pyrolytic graphite. It appears that the saturation ratio is slightly decreased in a-C:W, compared to pyrolytic graphite. At a fluence of 10^{19} D/cm^2 the D inventory in 7.5% a-C:W is also lowered by about $1 \cdot 10^{16}$ D/cm^2 compared to the D inventory in pyrolytic graphite. In the fluence range between 10^{17} D/cm^2 and 10^{19} D/cm^2, the increase of the D inventory of a-C and a-C:W (2.5% and 7.5%) can not be distinguished from the increase of the D inventory of pyrolytic graphite. a-C, 2.5% a-C:W and 7.5% a-C:W do not exhibit a significantly changed retention behaviour up to a fluence of 10^{19} D/cm^2 compared to the pyrolytic graphite.

Above 10^{19} D/cm^2, the D inventory depends strongly on the W concentration. For 2.5% a-C:W the D amount rises to higher values at a fluence of 10^{20} D/cm^2 compared to pyrolytic graphite. In contrast, for 7.5% a-C:W the amount of retained D is reduced to the half value of pyrolytic graphite at a fluence of 10^{20} D/cm^2. Both effects, the increase of the D inventory for 2.5% a-C:W and the decrease of the D inventory for 7.5% a-C:W, above a fluence of 10^{19} D/cm^2, are reproducible. Note it appears that data points of 7.5% a-C:W follow a curve, which shows a minimum at a fluence of $8 \cdot 10^{19}$ D/cm^2 and increases again above this minimum with further increasing fluence. The curve proceeding, however, must be presumed as a trend, since the difference of the D inventory of neighbouring data points is not significant, within the accuracy of 10%. For a-C,

however, the D inventory increases monotonically above a fluence of 10^{19} D/cm^2. Therefore, it is possible to compare results with results obtained for pyrolytic graphite by the magnitude X in the power law Φ^X, in the fluence range between 10^{17} D/cm^2 and 10^{20} D/cm^2. The magnitude X results in a value of 0.12 ± 0.01 for a-C. This value can not be distinguished from the value obtained for pyrolytic graphite, which has an error bar of $\pm$ 0.02.

Note that in [25] only two data points exist for the 7.5% a-C:W, i.e., at a fluence of 10^{17} D/cm^2 and at a fluence of 10^{20} D/cm^2. In the mean time, the fluence range in between was filled by additional data points. So, the resulting curve is different to that fluence dependence of the D inventory of 7.5% a-C:W, which was suggested in [25] to follow $\Phi^{0.05}$. An explanation for this difference may be given by the influence of the W enrichment zone on the increase of the D inventory with fluence, which will be discussed in section 4.2

3.3.2 D inventory of enriched a-C:W at 300 K

For studying the influence of the W enrichment zone on the fluence dependence of the D inventory, 7.5% a-C:W were exposed to a 200 eV D beam at 300 K and at a fluence of 10^{20} D/cm^2, to create a W enrichment zone in steady state (see section 4.1.2). Then these enriched 7.5% a-C:W were in-situ outgased at 1300 K. These enriched 7.5% a-C:W were implanted in the 2^{nd} run of a D beam exposure at 300 K and at different fluences between 10^{16} D/cm^2 and 10^{20} D/cm^2, and the retained amount was measured. NRA measurements on an outgased specimen, before the 2^{nd} exposure to the D beam, showed that $\sim$0.1% of the D from the first run remained in the films. This amount can be neglected compared to the inventory after the 2^{nd} exposure to the D beam.

The D inventories of the 2^{nd} exposure are given in figure 5, labeled as the *enriched 7.5% a-C:W*. At fluences below 10^{16} D/cm^2, the reflection coefficient seems to be close to 55%, i.e., the value for W. At a fluence of 10^{16} D/cm^2 and above, the D inventory tends to follow a curve rather than a line. Since the data point at a fluence of 10^{16} D/cm^2 is still close to the dashed line, the

implantation zone appears to become saturated with D at this fluence. The D content in the saturated implantation zone of the enriched 7.5% a-C:W (saturation level of $\sim 3 - 6 \cdot 10^{15}$ D/cm^2) is nearly an order of magnitude lower than the D content in the saturated implantation zone of the non-enriched 7.5% a-C:W. This leads to a saturation ratio of D/W of 0.03 - 0.15, assuming an amount of W in the enrichment zone of $40 - 100 \cdot 10^{15}$ at/cm^2. This means, the saturation behaviour inside the implantation zone is dominated by W. At fluences above 10^{16} D/cm^2, however, the D inventory increases with fluence, but does not reach a limit.

3.3.3 Binding energy in a-C:W

Thermal desorption spectroscopy (TDS) was performed in order to compare the trapping behaviour of a-C and a-C:W, regarding the influence of C bondings in the vicinity of a W carbide bonding and the influence of the enrichment. The trapping behaviour of a-C and a-C:W will be compared to the respective trends observed for fluence dependences of the D retention, especially above a fluence of 10^{19} D/cm^2.

Regarding the interpretation of the TDS spectra, the temperature axis is supposed to depend only on the bonding energies, without taking the effect of diffusion on the position of peaks into account. In figure 6 (a) /(b) a concentration series of the temperature dependence of the D_2 and the CD_4 signal for a-C and a-C:W, implanted at 10^{20} D/cm^2, is depicted (in (a): D_2 amount, in (b): CD_4 amount).

Regarding the D_2 signal (figure 6 (a)), the peak maximum shifts to lower temperatures for a-C:W (up to $\sim$200 K compared to a-C). The maximum decreases from $\sim$900 K to $\sim$850 K increasing the W concentration from 2.5% to 7.5%, i.e., D was bonded at lower energies. Regarding the peak widths of the concentration series, 7.5% a-C:W shows the lowest value ($\sim$300 K); only a small range of bonding energies was occupied. The peak width of a-C ($\sim$400 K) is larger and thus a larger range of bonding energies was occupied. The largest peak width among the a-C:W are obtained for 2.5% a-C:W ($\sim$400 K), including ranges of binding energies of a-C and 7.5 % a-

C:W. For 2.5 % a-C:W both W like and C like ranges of bonding energies were occupied. This is in convolution with a large amount of retained D, observed in 2.5% a-C:W, and a low amount observed in 7.5% a-C:W, at a fluence of 10^{20} D/cm^2.

Figure 7 shows the temperature dependence of the D_2 signal for (a) a-C, (b) 2.5% a-C:W, (c) 7.5% a-C:W, implanted at different fluences (10^{17} D/cm^2, 10^{19} D/cm^2 and 10^{20} D/cm^2). A rather weak change of the peak width with increasing fluence is observed for a-C. For a-C an increase of the D inventory with fluence is observable as an increase of the signal intensity along the entire temperature range. For a-C:W, on the other hand, the peak width changes with increasing fluence, besides the increase of the signal intensity with fluence. Increasing the fluence from 10^{19} D/cm^2 to 10^{20} D/cm^2, the peak width increases for 2.5% a-C:W and it decreases for 7.5% a-C:W. This is in convolution with an increase of the D inventory for 2.5% a-C:W and in a decreases of the D inventory for 7.5% a-C:W. Note that the origin of the spike at $\sim$1050 K for 7.5% a-C:W (of the milder spikes for 1% a-C:W and 2.5% a-C:W as well) is not known yet.

In addition to the D_2 signal, the CD_4 signal was recorded for all specimens mentioned above (figure 6 (b)). The release of methane is one of the reaction steps described in Küppers cycle [37–39]. This step describes a transition from a hydrogenated sp^3 bond to a sp^2 bond between C atoms, which is thermally activated and occurs in absence of the D beam.

With increasing W concentration, the maximum of the CD_4 signal shifts to lower temperatures, by about 200 K. In general, peak intensities of the CD_4 signals obtain lower values compared to the D_2 signal (between 1/3 and 1/10). Peaks are symmetric and extended over a smaller temperature range. The temperature difference between peak maximums is smaller. Despite these minor differences, trends observed for the D_2 signal were observed for the CD_4 signal, too. The peak maximum shifts to lower temperatures with increasing W concentration, indicating a lowering of the activation energy of the methane release. The total amount of released methane decreases with increasing W concentration as well.

3.4 Influence of temperature on D inventory

Concerning the D retention behaviour, the influence of temperature on the increase of the D inventory with fluence was investigated for a-C and 7.5% a-C:W.

3.4.1 Temperature series of fluence dependence of D inventory

Figure 8 shows a temperature series between 300 K and 1300 K of the amount of retained D, n_D, a as function of the fluence Φ of incident D for 7.5% a-C:W. Additionally, a solid line through the origin is shown, which has a slope of 100%.

At 300 K, data points are connected, which illustrates the curve shape already described in section 3.3. At 500 K two data points are given, at a fluence of 10^{17} D/cm^2 and of 10^{20} D/cm^2, which match the data at 300 K. This leads to the assumption that the inventory in the saturated implantation zone is at 500 K not different to 300 K and, further to this, that the inventory decreases again above a fluence of 10^{19} D/cm^2 by the loss of bonded D through the emission of volatile hydrocarbons, as previously observed at 300 K.

At 700 K the D inventory obtains lower values in the fluence range between $\sim 5 \cdot 10^{15}$ D/cm^2 and 10^{20} D/cm^2. Data points given at fluences between $\sim 5 \cdot 10^{15}$ D/cm^2 and $1 \cdot 10^{17}$ D/cm^2 do not follow the line through the origin, but rather a curve. With increasing fluence the D inventory increases along this curve and the gradient of the curve decreases. So the implantation zone appears to become saturated at fluences between $\sim 5 \cdot 10^{15}$ D/cm^2 and $1 \cdot 10^{17}$ D/cm^2. However, it can not be decided from the data, at which fluence saturation of the implantation zone is finally completed. Therefore, no fixed value can be given for the saturation level; rather a range must be given: $6 \cdot 10^{15}$ - $2 \cdot 10^{16}$ D/cm^2. For fluences above 10^{17} D/cm^2 the increase of the D inventory with fluence can be described by a power law Φ^X, in good agreement with the experimental data. The exponent X over the fluence Φ obtains a value of 0.12, which is in agreement of the value

for a-C at 300 K. Note that this only holds, if the implantation zone is saturated at 10^{17} D/cm^2. If saturation was completed already at lower fluences, the D inventory would increase stronger with fluence at 700 K, compared to 300 K. The decrease of the D inventory for fluences above 10^{19} D/cm^2, on the other hand, which is observable at 300 K, is not observable at 700 K. Due to the low number of data points given it can not be decided, whether this lowering is less pronounced or even does not exist at 700 K. Nevertheless, if the data point at a fluence of 10^{20} D/cm^2 obtained a lower inventory due to enrichment, compared to the inventory at a fluence of e.g. 10^{19} D/cm^2, the D inventory would increase stronger with fluence (i.e., for fluences below 10^{19} D/cm^2) than at 300 K. Altogether, it is suggested that the D inventory increases stronger with fluence at 700 K than at 300 K. Therefore, the diffusion of D would be enhanced at 700 K, which was already observed from the depth profiles of D (see section 3.2.2).

Above 700 K, it is not possible to describe the increase of the D inventory with fluence by a power law. Specifically at high fluences, data points can not be related to this kind of curve progression, since the D inventory shows a non-monotonic increase with fluence, which is becoming very pronounced with increasing temperature. At 900 K, the D inventory shows a minimum at fluences of 10^{19} - 10^{20} D/cm^2. Increasing the fluence from 10^{19} D/cm^2 to $5{\cdot}10^{19}$ D/cm^2 the D inventory decreases more than a half order of magnitude from a level of 10^{17} D/cm^2 to $4{\cdot}10^{16}$ D/cm^2. Increasing the fluence further to 10^{20} D/cm^2 increases the D inventory again to a level close to 10^{17} D/cm^2. At 1100 K, two data points exist at fluences around $\sim 10^{20}$ D/cm^2, which exhibit a lowered D inventory compared to the data point at a fluence of 10^{19} D/cm^2. This decrease is in line with the decrease already observed at 300 K and at 900 K, and confirms that these values can not be interpreted as runaway values. Note that data evaluation performed in the manner described in [25], leads to an accuracy of 10% for the D inventory and to an accuracy of 16% for the fluence of incident D. In figure 8, both error bars are added to data points obtained at 900 K. Further to this, it was ensured that the influence of temperature on trapping and diffusion of D does not result in a discrepancy between the measured D inventory and the D inventory at the very moment of the switch off of the D beam. For each implantation at elevated temperatures heating of the specimen was stopped $\sim$0.5 s after the switch off of the D beam.

It is known from a cross-checking experiment that D does not effuse from the specimen at implantation temperature, after the switch off of the D beam (see section 3.2). From this result, an effusion of D from the specimen can be excluded for at least a further 36 s of heat treatment at constant temperature after the D beam exposure.

Since the respective fluence ranges can not be related to the underlaying processes, for implantation temperatures above 700 K, only trends can be observed. Curves in the graph are a guide to the eye and try to illustrate overall trends for the saturation level and the increase of the D inventory with fluence. Increasing the temperature from 700 K to 1100 K shows that trends already observed at lower temperatures are continued. At 900 K the D inventory obtains lower values compared to the case at 700 K for fluences below 10^{17} D/cm^2; the implantation zone is saturated at lower fluences. Above the D inventory increases stronger than at 300 K and thus obtains values above the level at 300 K, already at a fluence of 10^{18} D/cm^2; the whole curve progression is inclined. At 1100 K trends are even more pronounced. The lowering of the D inventory at low fluences is even stronger than at 900 K. This means, the implantation zone appears to become saturated already at very low fluences, outside the measurement range. At a fluence of 10^{19} D/cm^2, on the other hand, the D inventory obtains a value even larger than at 900 K.

3.4.2 Influence of W inclusions and of C structure on accumulation of D at 900 K

In a further step, the influence of W inclusions and the influence of the C structure on the D retention were investigated at 900 K. In figure 9, 7.5% a-C:W is compared to a-C and pyrolytic graphite after the D beam exposure at 900 K. Data obtained from implantations at 300 K are inserted for comparison. Since the specimens were heat treated at 1300 K, a-C and a-C:W have the same C structure [40]. Therefore, the influence of W is studied by comparing a-C:W with a-C and the influence of the C material is studied by comparing a-C with pyrolytic graphite.

The D inventory of a-C implanted at 900 K is shifted by about a half order of magnitude to higher values, compared to pyrolytic graphite. But the increase of the D inventory with fluence

for a-C and pyrolytic graphite can not be distinguished from each other.

Comparing a-C and 7.5% a-C:W, implanted at 900 K, shows that the D inventory of 7.5% a-C:W obtains the two-fold and the three-fold of the value of a-C at a fluence of 10^{17} D/cm^2 and of 10^{19} D/cm^2, respectivley. Therefore, the D inventory of a-C seems to exhibit a slightly decreased increase with fluence compared to 7.5% a-C:W. This means, W inclusions lead to an intrinsic change of the D retention behaviour at an implantation temperature of 900 K, which is in contrast to the behaviour observed at 300 K, where all three materials exhibit the same behaviour except around 10^{19} D/cm^2.

4 Discussion

The tungsten enrichment affects the deuterium retention behaviour. Therefore, the retention behaviour is discussed taking results from the investigations of the W enrichment into account.

4.1 Enrichment of W under D beam exposure

4.1.1 Influence of temperature on W enrichment

From the increase of the width of the enrichment zone at elevated temperatures far above the width of the ion range, the question is raised whether it is possible to remove carbon (C) in the form of volatile hydrocarbons from the whole depth, which matches the width of the enrichment zone. C is removed from depths, which are not reached by energetic D. Therefore, one or several processes must be thermally activated, which enable D and C to get in contact and thus to react with each other. Two possibilities are discussed in the following:

If D and C get into contact and react with each other beyond the width of the ion range, one can assume that thermalised D diffuses into depth and reacts with the undamaged C matrix, i.e., that the thermal chemical erosion occurs at the undamaged C beyond the width of the ion

range. The reactivity of the undamaged C depends on structure, i.e., on the amount of open sp^2 sites. While undamaged pyrolytic graphite exhibits a yield for the thermal chemical erosion of an order of magnitude lower than pre-irradiated pyrolytic graphite, co-deposited C exhibits a yield for the thermal chemical erosion in the same order of magnitude as pre-irradiated pyrolytic graphite [41]. If a-C:W has a similar structure to co-deposited C, i.e., a similar amount of open sp^2 sites, the thermal chemical erosion is pronounced to a similar extent in the undamaged C matrix as within the width of the ion range. In this case, one would expect that C reacts with D over the entire diffusion depth of D, which extends up to 0.5 μm at 900 K, and thus that C is lost from depths up to 0.5 μm. From this point of view, however, it is unclear why the width of the W enrichment zone, which is 50 nm at 900 K, is considerably smaller than the observed diffusion depth of 0.5 μm at 900 K. This would mean that hydrocarbons are released from depths matching the width of the enrichment zone but retained at depths beyond the width of the enrichment zone. This problem, however, can not be clarified within the frame of this study.

Further to this, the question is raised whether a process may be thermally activated, which enables energetic D to get in contact with C from the depth. If energetic D can not reach C in the depth, C from the depth must diffuse towards the width of the ion range. In literature studies exist, which examine thermal activated diffusion of C into W [42,43]; note that these studies were not performed on a-C:W. In both studies, an increasing amount of C atoms diffused through W into depth with increasing temperature. These examples show that thermally activated processes were observed, in a system similar to a-C:W covered by a W enrichment zone. So, this result may be transferable to the case of the formation of a W enrichment zone in a-C:W during the D beam exposure at elevated temperatures. As soon as W is temporarily enriched over the width of the ion range, the C concentration gradient may drive a diffusion of C, which is thermally activated. In this case the temperature range, which exhibits a growing width of the enrichment zone (above 700 K), would correspond to a temperature range, which exhibits an enhanced diffusion of C in W.

4.1.2 Influence of W concentration on W enrichment at 300 K

For a-C:W exposed to a 200 eV D beam at 300 K and at a fluence of 10^{20} D/cm^2 it was shown that the total yield of removed C is significantly reduced compared to pure carbon films (a-C) [24]. This reduction is less sensitive on the W concentration and insensitive to the heat treatment before the D beam exposure [24].

In literature two explanations can be found for a reduction of the total yield of C in metal-containing carbon, a changed chemistry between C and D [44–47], on one hand, and the shielding effect [23,45,48], on the other hand. The shielding effect, however, is the most widely used explanation for a reduction of the total yield of removed C in metal-containing carbon [23,45,48]. This effect suggests a fluence dependence of the erosion yield until a steady state is reached.

In this context the question raises, for which specimen from the concentration series, which was obtained at 300 K in [24], it can be expected that - already at a fluence of 10^{20} D/cm^2 - erosion and retention behaviour are considerably affected by the presence of a W enrichment zone in steady state. The fluence necessary to reach steady state for a specimen from the concentration series, however, is not known. But it is possible to calculate a minimum amount of C, which needs to be removed to reach steady state. If this minimum amount is larger than the measured amount of removed C at a fluence of 10^{20} D/cm^2 (see [24]), it can be concluded that steady state has not been reached. In steady state, the width of the enrichment zone and the W concentration do not change with fluence of incident D, i.e., the enrichment zone contains a certain amount of W atoms. By taking the amount of W atoms in the enrichment zone and the initial W concentration into account, it is possible to calculate a minimum amount of removed C at steady state.

In table 1 values obtained for the minimum amount of removed C at steady state are compared to measured amounts of removed C at 300 K for the different W concentrations (taken from [24]).

For a 200 eV D beam, which contains 5% of 1.2 keV neutrals, steady state has not been reached for the W concentrations of 2.5% and below. Above 2.5%, however, it can not be concluded

Initial W content (%)	1	2.5	4	6	7.5	15
Amount of removed C (10^{17} at/cm^2)						
- measured at 10^{20} D/cm^2 [24]	19	19	31	31	23	18
- minimum at steady state (1.2 keV D)	100	40	25	17	13	7

Table 1

Comparison of the minimum amount of C to be removed to reach steady state to the measured amount of removed C at a fluence of 10^{20} D/cm^2 and at 300 K(see [24]). Multiple data points at a concentration were averaged.

whether steady state has been reached, since the physical sputtering yield of W is considerable around 1 keV [15]. Therefore, additional amounts of C need to be removed to reach steady state. The additional amount of removed C depends on the fluence, which needs to be accumulated to reach steady state.

This result needs to be compared to results obtained from the analysis of the width and the composition of the W enrichment zone (see section 3.1). For 7.5% a-C:W exposed to a 200 eV D beam (containing 5% 1.2 keV neutral particles) at 300 K and at a fluence of 10^{20} D/cm^2 it was shown that the W concentration in the enrichment zone is close to 100% and that the width of the enrichment zone matches the width of the ion range; an enrichment zone has formed, which is in steady state.

Altogether, from the analysis of the W enrichment zone and from the estimations mentioned above it is known that for the W concentrations of 2.5% and below, the enrichment zone is not in steady state, and that for the W concentrations of 7.5% and above, the W enrichment zone is in steady state at a fluence of 10^{20} D/cm^2 (and at 300 K).

4.2 Influence of W on accumulation of D at 300 K

From a comparison of the fluence dependence of the D inventory (under the 200 eV D beam exposure at 300 K) of a-C and a-C:W with the fluence dependence of the D inventory of pyrolytic graphite it could be shown that the D retention behaviour of a-C and a-C:W is, in principal, determined by the same processes, which are well known in literature to occur in graphites. In the following the intrinsic effect of W and the effect of W enrichment on these processes will be discussed.

4.2.1 Increase of the D inventory with fluence - Diffusion of D into depth

Above a fluence of $1 \cdot 10^{17}$ D/cm^2, the increase of the D inventory with fluence in a-C is interpreted to be caused by the diffusion of D into depth. It can be excluded from AFM analysis (see appendix A) that roughening causes this increase of the D inventory with fluence. By applying AFM it was shown that the difference of surface roughness for the different W concentrations (i.e. the a-C:W implanted at a fluence of 10^{19} D/cm^2) is even slightly above the extent of roughening with increasing fluence in a-C (increasing the fluence from 10^{19} D/cm^2 to 10^{20} D/cm^2). At a fluence of 10^{19} D/cm^2, however, the D inventory can not be distinguished for the different W concentrations. Therefore, differences of surface roughness in those magnitudes given in appendix A do not influence the D inventory. This observation must also be valid for increasing the fluence on a-C from 10^{19} D/cm^2 to 10^{20} D/cm^2.

As-deposited a-C and a-C:W exhibit about the same increase of the D inventory with fluence as pyrolytic graphite for fluences below 10^{19} D/cm^2. By the TDS measurements it was shown that W promotes the release of D at lower temperatures, in molecular form as well as bonded in deuterated methane. This indicates an intrinsically changed trapping behaviour for a-C:W. Nevertheless, an intrinsically changed trapping behaviour does not result in a changed increase of the D inventory with fluence at 300 K and at fluences below 10^{19} D/cm^2.

By applying TDS measurements, a fluence dependence of the trapping behaviour of a-C:W was observed and it is possible to identify changes in the trapping behaviour with fluence as cause for the fluence dependence of the D retention. For fluences of 10^{19} D/cm^2 and below all materials show a common property: Unoccupied bonding states are occupied with increasing fluence, which is observable as an increase of the overall intensity of the D_2 signal in all TDS spectra. The occupation of unoccupied bonding states certainly enables the total amount of retained D to increase with fluence. At fluences between 10^{17} D/cm^2 and 10^{19} D/cm^2, when all bonding states in the implantation zone are occupied, further occupation of bonding states occurs at larger depths. This requires the diffusion of D into depth. In this case, the diffusion of D into depth at 300 K is not different between a C material, which exhibits a graphite structure (pyrolytic graphite), and a C material, which exhibits an amorphous structure (a-C). Furthermore, the diffusion of D into depth is not affected by the W inclusions and thus by a changed trapping behaviour observed in a-C:W.

4.2.2 Increase of the D inventory with fluence - Enrichment

For fluences between 10^{19} D/cm^2 and 10^{20} D/cm^2 the increase of the D inventory with fluence in a-C:W is not dominated by the diffusion of D into depth. In this fluence range the increase of the D inventory depends strongly on the W concentration. For the concentration dependence of the D inventory an explanation can be given by TDS experiments, by analyses of surface roughness as well as by analyses of the W enrichment zone.

By TDS experiments it was possible to compare the energy range of bonding states, which are occupied with D in a-C and a-C:W. In 2.5% a-C:W the energy range of occupied bonding states has the same magnitude as in a-C. In 7.5% a-C:W it is decreased below the range in a-C.

For 2.5% a-C:W surface roughness increases clearly with increasing fluence from 10^{19} D/cm^2 to 10^{20} D/cm^2, which is observable as an increase of the RMS value and the surface area to the 10-fold and to the 1.17-fold, respectively. An increase of the surface area to the 1.17-fold

leads to an increase of the implantation volume by the same factor. This increase, however, is not sufficient to explain the doubling of the D inventory with fluence. Another explanation may be given by the erosion behaviour. It was shown that the total yield of C is clearly reduced in 1% a-C:W and 2.5% a-C:W compared to a-C [24]. Additionally, it was shown that the enrichment zone is not in steady state at a fluence of 10^{20} D/cm^2 for 1% a-C:W and 2.5% a-C:W, which is also observable in an enlarged magnitude of the energy range of occupied bonding states (i.e., it covers the range observed in TDS spectra for a-C as well as the range observed for 7.5% a-C:W). This means that an enlarged amount of bonded D is present, of which only low portions are released through the formation of volatile hydrocarbons. Major portions are trapped, which leads to a strong increase of the D inventory.

For 7.5% a-C:W the RMS value and the surface area decrease with increasing fluence (10^{19} D/cm^2 - 10^{20} D/cm^2) to the 0.65-fold (from 3.7 nm to 2.4 nm) and to the 0.98-fold (from 4.14 μ m^2 to 4.05 μ m^2), respectively. But this does not explain the reduction of the D inventory. Similarly to the situation mentioned for a-C, small changes in surface roughness with fluence do not lead to a change of the D inventory. In fact, for 7.5% a-C:W a surface enriched to 100% W is formed over the width of the ion range, increasing the fluence from 10^{19} D/cm^2 to 10^{20} D/cm^2. This may be confirmed by the following assessment: Under the assumption that an averaged C erosion yield of $\sim$2% (see [24]; 7.5% a-C:W) is close to the erosion yield at a fluence of 10^{19} D/cm^2, a C layer of about 20 nm would have been removed at a fluence of 10^{19} D/cm^2, leaving behind a W enrichment zone with a width of about 2 nm. Since the width of the ion range is 5.5 nm in pure C and 6.3 nm in pure W, for a 200 eV/D beam, D atoms are able to reach the unaffected C matrix, where they are trapped at a D/C ration of 0.4. At a fluence of 10^{20} D/cm^2 the W enrichment zone is in steady state for 7.5% a-C:W. The width of the enrichment zone matches the width of the ion range; the W concentration is close to 100% (see section 4.1.2). In this case the impacting D beam is stopped and thermalised inside the enrichment zone and - neglecting diffusion into depth - bonded to W atoms, where the ratio of D/W is reduced. This difference matches the lowering of the inventory at fluences of 10^{20} D/cm^2. (Note, in the TDS spectra it can be observed that the build-up of an enrichment zone at fluences of 10^{19} - 10^{20} D/cm^2, and

the successive removal of C atoms leads to a release of D from occupied bonding states through the formation of volatile hydrocarbons, i.e., mainly from high energetic bonding states.)

4.2.3 Increase of the D inventory with fluence - Extrapolation

The most obvious effect of W inclusions on the accumulation of D in a-C:W lies in the enrichment of W at fluences above 10^{19} D/cm^2. At fluences between 10^{19} D/cm^2 and 10^{20} D/cm^2, the evolution of an enrichment zone changes the D inventory in a-C:W compared to a-C. In ITER a fluence of 10^{20} D/cm^2 will be reached at baffle and dome after about 25 of 400 s ITER-discharges and at the vertical target after about a second. So, concerning the effect of enrichment on the increase of the D inventory with fluence and its relevance for ITER, a fluence range far above 10^{20} D/cm^2 is of major interest. For such high fluences it can be assumed that the enrichment zone is already in steady state, in a-C:W, without respect to the W concentration. In this case, D is implanted into enriched a-C:W.

In this study the retention behaviour of enriched a-C:W was investigated at 300 K and for fluences between 10^{16} D/cm^2 and 10^{20} D/cm^2. For the enriched a-C:W the reflection coefficient is close to the value of W (55%) and the saturation ratio inside the implantation zone is lowered to 0.03 - 0.15. Nevertheless, for the enriched 7.5% a-C:W the D inventory still increases for fluences above saturation of the implantation zone (above 10^{16} D/cm^2). In [49] a W film of 200 nm thickness, deposited on graphite, was exposed in the Garching high current ion source to the D beam at 200 eV/D and at 300 K. It was shown that the saturation ratio of D/W in amorphous W is not larger than 0.06 within the width of the ion range in W. Note that a similar saturation ratio was also found in bulk tungsten [50]. Therefore, for a W enrichment zone of a width of $40 - 100 \cdot 10^{15}$ at/cm^2, which equals the width of the ion range between 200 eV/D and 1.2 keV/D, the D amount saturates at $2.4 - 6 \cdot 10^{15}$ D/cm^2. Therefore, the increase of the D inventory in the enriched 7.5% a-C:W above this level with increasing fluence appears to be due to the diffusion of D into depths beyond the width of the enrichment zone. It appears that W at the surface can not hinder D to diffuse into depth. In other words, for an evolution of the enrichment zone

close to steady state, the influence of diffusion into depth on the increase of the D inventory with fluence appears to become dominant over the influence of enrichment and of the trapping behaviour inside the enrichment zone. Therefore, the increase of the D inventory with fluence appears to become dominated again by the retention behaviour of the unaffected C matrix in the depth for 7.5% a-C:W at fluences above 10^{20} D/cm^2.

It was suggested that the diffusion of D into depth is not different in a-C:W compared to a-C and pyrolytic graphite for fluences below 10^{19} D/cm^2. If the increase of the D inventory with fluence in a-C:W, above a fluence of 10^{20} D/cm^2, is dominated by diffusion through the unaffected C matrix, it is suggested that diffusion into depth and the increase of the D inventory with fluence are not different in a-C:W and in a-C for fluences above 10^{20} D/cm^2, too. Therefore, the difference of the D inventory between a-C and a-C:W is supposed to be limited to a small fluence range around 10^{20} D/cm^2, and thus the increase of the D inventory with fluence in a-C:W can be described by the power law Φ^X for very large fluences. The exponent X must be the same in a-C and a-C:W. For a-C the exponent X was verified to be 0.1.

4.3 Influence of implantation temperature on accumulation of D

The influence of implantation temperature on the diffusion of D into depth was studied in a cross-checking experiment (see subsection 3.2.1). The most important interpretation is that the diffusion of D into depth and the number of available bonding states are in convolution with each other. With increasing temperature the number of available bonding states decreases. An enlarged number of bonding states enables thermalised D to be trapped inside the width of the ion range and slightly beyond. A low number of available bonding states forces thermalised D to diffuse - by the impact of the incoming D beam, which produces a concentration gradient - beyond the width of the implantation zone into depth ($\sim$90% of the total inventory at 900 K and at a fluence of 10^{18} D/cm^2). An increased implantation temperature leads to a decreased number of available bonding states (i.e. a lowered saturation ratio in the implantation zone) and to an increased diffusion into depth.

The influence of temperature on the saturation ratio in the implantation zone and on the diffusion depth is quantifiable for 7.5% a-C:W implanted at temperatures between 300 K and 900 K and at a fluence of $\sim 10^{20}$ D/cm^2. For the maximal diffusion depth at 300 K (60 nm), which is only slightly above the resolvable depth, an average D concentration of 0.05 is given. If the total amount of the retained D was trapped within the implantation zone (within $\sim$10 nm), the D concentration within the implantation zone would be the six-fold of the D concentration within the diffusion depth, i.e., 0.3. This corresponds to a value of 0.43 for the ratio of D/C, which is about in agreement with the value of 0.4 for the saturation ratio of D/C inside the implantation zone well known in literature [51]. In the medium temperature range between 700 K and 900 K, it is possible to distinguish between D trapped below the resolvable depth and D trapped at depths larger than the resolvable depth. At 700 K, 50% of the D inventory is trapped within 60 nm below the surface and obtains a concentration of 0.02. If this D inventory was trapped inside the implantation zone, one would obtain a value of 0.2 for the ratio of D/C. Therefore, the saturation ratio of D/C in the implantation zone is lowered at 700 K compared to 300 K.

Further to this, an increased diffusion into depth is in convolution with an enhanced increase of the D inventory with fluence at high implantation temperatures. Both are the most obvious effects of the implantation temperature on the retention behaviour of a-C:W. If the increase of the D inventory with fluence was caused by the diffusion of D into depth, an explanation can be found for the overall trends observed concerning the D retention behaviour in a-C:W at elevated temperatures, by relating the diffusion of D into depth and thus the increase of the D inventory with fluence to the number of available bonding states, which depends on temperature.

This interpretation can also explain the intrinsic effect of W on the retention behaviour of a-C:W at elevated temperatures. The intrinsic effect of W was investigated by comparing the retention behaviour of 7.5% a-C:W and a-C at 900 K. For 7.5% a-C:W the increase of the D inventory with fluence is slightly enhanced compared to a-C. Furthermore, in the spectrum of the D_2 signal obtained by TDS, the maximum is shifted by about 200 K, from 1050 K for a-C to 850 K for 7.5% a-C:W, i.e., just below 900 K; in 7.5% a-C:W the number of available bonding states is

lower at 900 K than in a-C. From the interpretation made above, this must lead to an enhanced diffusion depth in 7.5% a-C:W and to an enhanced increase of the D inventory with fluence. Consequently, the intrinsic effect of W on retention can be explained by the changed number of available bonding states and thus by the changed trapping behaviour of 7.5% a-C:W.

Nevertheless, the changed trapping behaviour of 7.5% a-C:W can not explain the non-monotonic increase of the D inventory with fluence at fluences above 10^{19} D/cm^2, which is observable at temperatures above 700 K. This behaviour is difficult to explain.

In fact, enrichment of W is an issue, which must be addressed in trying to find a possible influence on the retention behaviour of 7.5% a-C:W at fluences above 10^{19} D/cm^2. As already discussed, at 300 K the enrichment of W in 7.5% a-C:W leads to a decrease of the D inventory with fluence, for fluences above 10^{19} D/cm^2. D bonded to C inside the implantation zone is lost in the form of volatile hydrocarbons during enrichment and an enrichment zone, containing 100% W, is left in steady state. A decrease of the D inventory for fluences above 10^{19} D/cm^2 is observable for 7.5% a-C:W, exposed to the D beam at 500 K, at 900 K and at 1100 K, too. (Note that this behaviour is not observable for the data given at 700 K.) From the analysis of W enrichment at 500 K it is known that the enrichment zone is in steady state at a fluence of 10^{20} D/cm^2, containing 100% W over depths, matching the width of the ion range. In consequence, D is lost by the formation of volatile hydrocarbons during W enrichment. At 500 K W enrichment dominates the retention behaviour of 7.5% a-C:W, in a fluence range between 10^{19} D/cm^2 and 10^{20} D/cm^2. For implantations at 900 K and above, however, it is not clear whether this kind of decrease of the D inventory is due to the enrichment of W. From the analysis of the W enrichment zone of the specimens implanted at a fluence of $\sim 10^{20}$ D/cm^2 it is not known whether steady state has been reached. (Note that at elevated temperatures an additional process occurs, which influences the composition of the W enrichment zone, i.e., the diffusion of C from the depth towards the shallow enrichment zone.) This information is necessary in order to decide for which data point between 10^{19} D/cm^2 and 10^{20} D/cm^2 steady-state is not reached and thus the loss of D is still under progress. Therefore, it is not possible to relate the proceeding of the

curves at 900 K and above to the proceeding of W enrichment, as it is possible at 300 K, and it remains unclear whether W enrichment influences the retention behaviour at fluences above 10^{19} D/cm^2 in the same way as it was observed at 300 K, i.e., through the loss of D bonded to volatile hydrocarbons.

5 Summary

Retention and enrichment of a model system for mixed layers, tungsten-containing carbon films (a-C:W), were investigated with respect to the interaction with deuterium ions. The use of a well-defined model system and the exposure to a mass-separated, mono-energetic D beam permitted quantitative investigations. The results are compared with the data for pure carbon films (a-C) and pyrolytic graphite.

The retention of a-C is at 300 K and 900 K no different to pyrolytic graphite. Above $\sim 10^{17}$ D/cm^2 the D inventory exhibits an increase with fluence Φ, according to Φ^X (e.g. x = 0.1 at 300 K and 0.23 at 900 K). The increase is interpreted to be driven by a diffusive process of D into depth, which is retarded by bonding processes between D and C. At 300 K and fluences up to 10^{19} D·cm^{-2}, the increase of the D inventory with fluence in a-C:W can not be distinguished from a-C and pyrolytic graphite. Therefore, the W inclusions do not affect the diffusion of D into depth. Above a fluence of 10^{19} D·cm^{-2}, however, the D inventory depends strongly on the W concentration. For 1% and 2.5% a-C:W, the surface strongly roughenes with increasing fluence. This leads to an enhanced implantation volume, which is supposed to result in the strong increase of the D inventory to the 1.5-fold of the D inventory of pyrolytic graphite at a fluence of 10^{20} D·cm^{-2}. For 7.5% a-C:W enrichment of W reduces the D inventory with increasing fluence; during erosion the D bonded to volatile hydrocarbons is lost so that the D inventory obtains the half value of pyrolytic graphite at a fluence of 10^{20} D·cm^{-2}.

For the temperature range between 300 K and 1300 K following trends can be observed: For each specimen from the temperature series the diffusion depth is larger than the width of the

W enrichment zone. In general, the D depth profiles showed that in a-C:W, D can diffuse into depths beyond the implantation zone. Furthermore, an increasing diffusion depth is in convolution with a rising increase of the D inventory with fluence with increasing temperature. However, the D inventory does not increase with fluence according to Φ^x, especially at fluences above 10^{19} D·cm^{-2}.

6 Conclusion

In a-C, in a-C:W and in pyrolytic graphite, the increase of the D inventory with fluence is interpreted to be based on the diffusion of D into depth. At 300 K and for fluences below 10^{19} D/cm^2, the extent of the diffusion of D into depth and thus the increase of the D inventory with fluence is not different in a-C:W compared to a-C and pyrolytic graphite. Above a fluence of 10^{19} D/cm^2, however, the D retention is dominated by the evolution of a W enrichment zone, which determines the saturation ratio in the implantation zone. Nevertheless, the build-up of a W enrichment zone is supposed to affect the D inventory in a closed range of fluence around 10^{20} D/cm^2. Outside this fluence range, a-C:W is supposed to exhibit the same D retention behaviour as pyrolytic graphite at 300 K so that an extrapolation of the increase of the hydrogen inventory with fluence to ITER-relevant fluence ranges appears to be uncritical for a-C:W. (Note that the increase of the hydrogen inventory with fluence does neither depend on particle energy and flux, for $\leq 10^{20}$ D/cm^{2}s [17], nor on the isotope species.)

By extrapolating the increase of the hydrogen inventory with fluence according to Φ^X (with X = 0.1 at 300 - 500 K) it can be shown that even after $0.5 \cdot 10^5$ 400 s ITER-discharges in the T burning phase, which fits the scheduled operation time of the T burning phase of 20 years, the T inventory in a-C:W - built up by implantation and diffusion into depth - is at 300 - 500 K two orders of magnitude below the safety limit of 700 g. This confirms that the build-up of the T inventory through the use of CFC is dominated at 300 - 500 K by the co-deposition of T and C in remote areas, as already well known in literature [4,20,52].

At elevated temperatures following trends were observed: The increase of the D inventory with fluence and the diffusion depth increase with temperature; the diffusion of D into depth is significant for temperatures at 700 K and above. Both trends are interpreted to be caused by the lowering of the number of available bonding states with increasing temperature.

A Surface morphology: Roughening

Processing of the data obtained from atomic force microscopy (AMF) was performed using the open-source software Gwyddion [53].

A.1 Roughening at 300 K versus W concentration

For the specimens exposed to the D beam at 300 K the roughening with increasing fluence was observed, e.g., at 10^{19} - 10^{20} D/cm^2. Thereby, the pure carbon film (a-C) was compared to the 2.5% and to the 7.5% tungsten-containing carbon film (a-C:W), by means of the root mean square value (RMS value) [54] and the surface area. For a-C the RMS value increases with increasing fluence to the 3.3-fold (from 1.1 nm to 3.6 nm). The surface area, however, is nearly constant (increase to the 1.01-fold, from 4.02 μ m^2 to 4.08 μ m^2). For 2.5% a-C:W the RMS value shows a strong increase with increasing fluence to the 10-fold (from 1.6 nm to 18 nm). The surface area also increases ssignificantly with increasing fluence to the 1.17-fold (from 4.10 μ m^2 to 4.81 μ m^2). For 7.5% a-C:W the RMS value decreases with increasing fluence to the 0.65-fold (from 3.7 nm to 2.4 nm). The surface area, however, is nearly constant (decrease to the 0.98-fold, from 4.14 μ m^2 to 4.05 μ m^2), respectively.

A.2 Roughening between 300 K and 1100 K

For the 7.5 a-C:W implanted at elevated temperatures the roughening with implantation temperature was observed. Only special features of surface roughness are of interest (the FWHM of

the surface roughness, the distribution of the local tilt angles of surface segments [29]), which are supposed to be important in the context of the resolvable depths, on one hand, and in the context of multiple surface crossings, on the other hand. (Note that a local tilt angle is obtained from the gradient between two neighbouring data points of the AFM line scans; the orientation of the line scans is chosen in that way so that the local tilt angle lies in the same plane as the incident and exit angle of the analysing beam used in the IBA experiments, which is determined by the geometry of the IBA set up.)

Surface roughness clearly changes with temperature. Above 900 K the FWHM of the surface roughness increases to 18.5 nm, from a nearly constant level between 300 K and 900 K (5 nm - 7 nm).

Figure A1 depicts the distribution of the local tilt angles of the temperature series of a-C:W by means of a relative frequency (each distribution was normalized to its maximum) plotted over tilt angles, between -40° and 40°. Vertical lines are inserted at the angle of $\pm 12°$ and at the angle of $\pm 20°$, respectively. (Note that these angles are determined by the geometry of the analysing beam in the NRA and RBS experiment, respectively.) If the FWHM is larger than the region, which is spanned by the vertical lines at $\pm 12°$ and at $\pm 20°$, it can be shown from the peak integrals that more than 10% among the local tilt angles are larger than $|12|°$ and $|20|°$, respectively. For this case it was defined that multiple surface crossings need to be taken into account in the NRA and in the RBS experiment, respectively. At 900 K and below, less than 10% among the local tilt angles are larger than $|12|°$ (at 700 K about 10% among the local tilt angles are larger than $|12|°$). Consequently, multiple surface crossings do not have to be taken into account for the specimens implanted at 900 K and below, neither in the RBS nor in the NRA spectra. At 1100 K, 27% among the local tilt angles are larger than $|12|°$ and 10% are larger than $|20|°$. Consequently, multiple surface crossings can only be neglected for the RBS spectrum.

2 Acknowledgements

The authors are grateful to Thomas Dürbeck for performing TDS measurements and for the fruitfull discussion about the evaluation of the TDS spectra, and to Wolfgang Jacob and Peng Wang for the fruitfull discussions. We are also grateful to Kazuyoshi Sugiyama for the data of the NRA analysis on tungsten coated graphites and fruitfull discussion.

References

[1] H. Bolt, V. Barabash, G. Federici, J. Linke, A. Loarte, J. Roth, and K. Sato. Plasma facing and high heat flux materials - needs for ITER and beyond. *J. Nucl. Mater.*, 307(Part A):43–52, 2002.

[2] P. Staib and G. Staudenmaier. Surface effects and impurity production in Tokamak machines. *J. Nucl. Mater.*, 76-7(1-2):78–91, 1978.

[3] R. Behrisch, M. Mayer, and C. GarciaRosales. Composition of the plasma facing material Tokamakium. *J. Nucl. Mater.*, 233(Part A):673–680, 1996.

[4] M. Mayer, R. Behrisch, H. Plank, J. Roth, G. Dollinger, and C.M. Frey. Codeposition of hydrogen with beryllium, carbon and tungsten. *J. Nucl. Mater.*, 230(1):67–73, 1996.

[5] P. Andrew, P.D. Brennan, J.P. Coad, J. Ehrenberg, M. Gadeberg, A. Gibson, D.L. Hillis, J. How, O.N. Jarvis, H. Jensen, R. Lasser, F. Marcus, R. Monk, P. Morgan, J. Orchard, A. Peacock, R. Pearce, M. Pick, A. Rossi, P. Schild, B. Schunke, and D. Stork. Tritium retention and clean-up in JET. *Fusion Eng. Des.*, 47:233–245, 1999.

[6] G. Federici, J.N. Brooks, D.P. Coster, G. Janeschitz, A. Kukuskhin, A. Loarte, H.D. Pacher, J. Stober, and C.H. Wu. Assessment of erosion and tritium codeposition in ITER-FEAT. *J. Nucl. Mater.*, 290:260–265, 2001.

[7] R. Behrisch, G. Federici, A. Kukushkin, and D. Reiter. Material erosion at the vessel walls of future fusion devices. *J. Nucl. Mater.*, 313:388–392, 2003.

[8] R. Kawakami, T. Shimada, Y. Ueda, and M. Nishikawa. Simulation study of dynamical material mixing on tungsten surfaces at elevated temperatures due to hydrogen and carbon mixed ion beam irradiation. *J. Nucl. Mater.*, 329(Part A):737–741, 2004.

[9] Y. Ueda, M. Fukumoto, I. Sawamura, D. Sakizono, T. Shimada, and M. Nishikawa. Carbon impurity behavior on plasma facing surface of tungsten. *Fusion Eng. Des.*, 81(1-7):233–239, 2006.

[10] M. Mayer, M. Andrzejczuk, R. Dux, E. Fortuna-Zalesna, A. Hakola, S. Koivuranta, K. Krieger, K. J. Kurzydlowski, J. Likonen, G. Matern, R. Neu, G. Ramos, M. Rasinski, V. Rohde, K. Sugiyama, A. Wiltner, W. Zielinski, and ASDEX-Upgrade Team. Tungsten erosion and redeposition in the all-tungsten divertor of ASDEX Upgrade. *Phys. Scr.*, T138:014039 (7pp), 2009.

[11] R. A. Pitts, A. Kukushkin, A. Loarte, A. Martin, M. Merola, C. E. Kessel, V. Komarov, and M. Shimada. Status and physics basis of the ITER divertor. *Phys. Scr.*, T138:014001 (10pp), 2009.

[12] T. Schwarz-Selinger, U. von Toussaint, C. Hopf, and W. Jacob. Fuel removal from tile gaps with oxygen discharges: Reactivity of neutrals. *Phys. Scr.*, T138:014009 (8pp), 2009.

[13] M. Balden. Characterization of nano-structured W-, Ti-, V-, and Zr-doped carbon films. *Thin Solid Films*, 519:4032–4036, 2011.

[14] J. Roth, E. Tsitrone, Th. Loarer, V. Philipps, S. Brezinsek, Al. Loarte, G.F. Counsell, R.P. Doerner, K. Schmid, O.V. Ogorodnikova, and R.A. Causey. Tritium inventory in ITER plasma-facing materials and tritium removal procedures. *Plasma Phys. Control Fus.*, 50(10), 2008.

[15] W. Eckstein, C. Garcia-Rosales, J. Roth, and W. Ottenberger. Sputtering Data. Techn. Rep. IPP 9/82, Max-Planck-Institut für Plasmaphysik, Garching, 1993.

[16] C. Adelhelm. *Structure and Erosion Behavior of Metal-doped Carbon Films*. PhD thesis, Technical University of Munich, 2008.

[17] J.W. Davis, A.A. Haasz, and D.S. Walsh. Flux and fluence dependence of H^+ trapping in graphite. *J. Nucl. Mater.*, 176:992–999, 1990.

[18] A.A. Haasz and J.W. Davis. Fluence dependence of deuterium trapping in graphite. *J. Nucl. Mater.*, 209(2):155–160, 1994.

[19] A.A. Haasz and J.W. Davis. Deuterium retention in doped graphites. *J. Nucl. Mater.*, 232(2-3):219–225, 1996.

[20] M. Mayer, M. Balden, and R. Behrisch. Deuterium retention in carbides and doped graphites. *J. Nucl. Mater.*, 252(1-2):55–62, 1998.

[21] M. Balden, E. Oyarzabal, E. de Juan Pardo, K. Durocher, J. Roth, and C. Garcia-Rosales. Deuterium retention by implantation in carbide-doped graphites. *Phys. Scr.*, T103:38–42, 2003.

[22] A.A. Haasz, P. Franzen, J.W. Davis, S. Chiu, and C.S. Pitcher. Two-region model for hydrogen trapping in and release from graphite. *J. Appl. Phys.*, 77(1):66–86, 1995.

[23] H. Plank and W. Eckstein. Preferential sputtering of carbides under deuterium irradiation - A comparison between experiment and computer simulation. *Nucl. Instrum. Methods Phys. Res., Sect. B*, 124(1):23–30, 1997.

[24] P. A. Sauter and M. Balden. Temperature dependence of the erosion behavior of deuterium beam exposed tungsten-doped carbon films (a-C:W) . *J. Nucl. Mater*, 415:S117–S120, 2011.

[25] P. A. Sauter and M. Balden. Deuterium retention in tungsten-doped carbon films. *Phys. Scr.*, T138:014044 (4pp), 2009.

[26] M. Balden, B.T. Cieciwa, I. Quintana, E.D. Pardo, F. Koch, M. Sikora, and B. Dubiel. Metal-doped carbon films obtained by magnetron sputtering. *Surf. Coat. Technol.*, 200(1-4):413–417, 2005. 9th International Conference on Plasma Surface Engineering, Garmisch Partenkirchen, GERMANY, SEP 13-17, 2004.

[27] W. Möller. Hydrogen trapping and transport in carbon. *J. Nucl. Mater.*, 162:138–150, 1989.

[28] W. Möller and F. Besenbacher. Note on the ^{3}He+D nuclear-reaction cross-section. *Nucl. Instrum. Methods*, 168(1-3):111–114, 1980.

[29] M Mayer. SIMNRA, a simulation program for the analysis of NRA, RBS and ERDA. Proceedings of the 15th International Conference on the Application of Accelerators in Research and Industry, J. L. Duggan and I.L. Morgan (eds.), American Institute of Physics Conference Proceedings 475, p. 541 (1999).

[30] M. Mayer. RESOLNRA: A new program for optimizing the achievable depth resolution of ion beam analysis methods. *Nucl. Instrum. Methods Phys. Res., Sect. B*, 266(8):1852–1857, 2008.

[31] M. Mayer. SIMNRA user's guide. Report IPP 9/113, Max-Planck-Institut für Plasmaphysik, Garching, Germany, 1997.

[32] E. Salancon, T. Duerbeck, T. Schwarz-Selinger, F. Genoese, and W. Jacob. Redeposition of amorphous hydrogenated carbon films during thermal decomposition. *J. Nucl. Mater.*, 376(2):160–168, 2008.

[33] W. Eckstein. Calculated Sputtering, Reflection and Range Values. Techn. Rep. IPP 9/132, Max-Planck-Institut für Plasmaphysik, Garching, 2002.

[34] J.R. Tesmer and M. Nastasi, editors. *Handbook of modern ion-beam materials analyses*. Materials Research Society, Pittsburgh, Pennsylvania, 1995.

[35] W. Eckstein. Reflection (Backscattering). Techn. Rep. IPP 17/12, Max-Planck-Institut für Plasmaphysik, Garching, 2009.

[36] C. H. Skinner, A. A. Haasz, V. KH. Alimow, N. Bekris, R. A. Causey, R. E. H. Clark, J. P. Coad, J. W. Davis, R. P. Doerner, M. Mayer, A. Pisarev, J. Roth, and T. Tanabe. Recent advances on hydrogen retention in ITER's plasma-facing materials: Beryllium, carbon, and tungsten. *Fusion Sci. Technol.*, 54(4):891–945, 2008.

[37] A. Schenk, B. Winter, J. Biener, C. Lutterloh, U.A. Schubert, and J. Küuppers. Growth and thermal-decomposition of ultrathin ion-beam deposited C:H films. *J. Appl. Phys.* , 77(6):2462–2473, 1995.

[38] J. Biener, U.A. Schubert, A. Schenk, B. Winter, C. Lutterloh, and J. Küppers. A surface reaction with atoms: Hydrogenation of sp-hybridized and sp2-hybridized carbon by thermal H(D) atoms. *J. Chem. Phys.*, 99(4):3125–3128, 1993.

[39] A. Horn, A. Schenk, J. Biener, B. Winter, C. Lutterloh, M. Wittmann, and J. Küppers. H atom impact induced chemical erosion reaction at C:H film surfaces. *Chem. Phys. Lett.*, 231(2-3):193–198, 1994.

[40] C. Adelhelm, M. Balden, M. Rinke, and M. Stueber. Influence of doping (Ti, V, Zr, W) and annealing on the sp(2) carbon structure of amorphous carbon films. *J. Appl. Phys.*, 105(3), 2009.

[41] J. Roth and C. Garcia-Rosales. Analytic description of the chemical erosion of graphite by hydrogen ions. *Nucl. Fusion*, 36(12):1647–1659, 1996.

[42] J. Luthin and Ch. Linsmeier. Carbon films and carbide formation on tungsten. *Surf. Sci.*, 454:78–82, 2000.

[43] K. Schmid. *Untersuchung der Temperaturabhängigkeit der Erosion von Wolfram durch Kohlenstoff*. PhD thesis, University of Bayreuth, 2002.

[44] V.K. Alimov, R. Schwörer, B.M.U. Scherzer, and J. Roth. Thermal-desorption of D2 and CD4 from bulk-boronized graphites. *J. Nucl. Mater.*, 187(3):191–196, 1992.

[45] M. Balden and C. Adelhelm. Characterization and erosion of metal-containing carbon films. *Phys. Scr.*, T128:121–126, 2007.

[46] J. Roth. Chemical erosion of carbon based materials in fusion devices. *J. Nucl. Mater.*, 266:51–57, 1999.

[47] R. Schwörer and J. Roth. Sputtering of boron-doped graphite USB15 - investigation of the origin of low chemical erosion. *J. Appl. Phys.*, 77(8):3812–3817, 1995.

[48] M. Balden, J. Roth, E. de Juan Pardo, and A. Wiltner. Chemical erosion of atomically dispersed doped hydrocarbon layers by deuterium. *J. Nucl. Mater.*, 313:348–353, 2003.

[49] K. Sugiyama. Personal communication. *Unpublished data*, 2011.

[50] A. Manhard, K. Schmid, M. Balden, and W. Jacob. Influence of the microstructure on the deuterium retention in tungsten. *J. Nucl. Mater.*, 415:S632–S635, 2011.

[51] W. Jacob and J. Roth. Chemical Sputtering. In R. Behrisch and W. Eckstein, editors, *Sputtering by Particle Bombardment, Experiments and Computer Calculations from Threshold to MeV Energies*. Springer, Berlin, 2006.

[52] R. Behrisch. Plasma-facing materials for fusion devices. *Journal of Surface Investigation-X-Ray Synchrotron and Neutron Techniques*, 4(4):549–562, 2010.

[53] D. Necas and P. Klapetek. Gwyddion: an open-source software for SPM data analysis. *Cent. Eur. J. Phys.*, 10(1):181–188, 2012.

[54] E.S. Gadelmawla, M.M. Koura, T.M.A. Maksoud, I.M. Elewa, and H.H. Soliman. Roughness parameters. *J. Mater. Process. Technol.*, 123(1):133–145, 2002.

Figure captions

Fig. 1):

Comparison of the width of the enrichment zone with the resolvable depth and the half value of the FWHM of the surface roughness in 7.5% a-C:W, exposed to a 200 eV D beam between 300 K and 1300 K and at 10^{20} D/cm^2.

Fig. 2):

NRA spectra of 7.5% a-C:W. All specimens were implanted with a 200 eV D beam at 900 K and at a fluence of 10^{18} D/cm^2. At this fluence either the heat treatment or the D beam exposure was continued for different time spans: In (a) D was implanted at additional fluences up to 10^{17} D/cm^2 (relaxiation time of cooling $\tau(1/e) \approx 90$ s), in (b) the heat treatment at 900 K was continued for different time spans up to 36 s and in (c) the temperature was increased once to 1100 K and after another exposure to 1300 K for 900 s. The amount of retained D, D_{tot}, as well as the specimen temperature at the end of the experiment are listed in the inserted tables.

Fig. 3):

The NRA spectra of 7.5% a-C:W, exposed to a 200 eV D beam between 300 K and 900 K and at 10^{20} D/cm^2.

Fig. 4):

The averaged D concentration (a) and diffusion depth (b) in 7.5% a-C:W, exposed to a 200 eV D beam between 300 K and 900 K and at 10^{20} D/cm^2; the resolvable depth is given in (a) for comparison. At 700 K two data points are given, respectively. The solid symbols describe the high energetic peak of the NRA spectrum (shown in the inlet of (a)) and the open symbols describe the tail towards lower energies.

Fig. 5):

Amount of retained D implanted at 300 K versus the fluence of incident 200 eV D for pyrolytic graphite, a-C and a-C:W ($\leq$7.5% W), and for the *W enriched a-C:W* at fluences between 10^{16} D/cm^2 and 10^{20} D/cm^2. Curves are a guide to the eye.

Fig. 6):

TDS spectra of (a) the D_2 signal and (b) the CD_4 signal of a-C and of a concentration series of a-C:W, which were exposed to a 200 eV D beam at 300 K and at a fluence of 10^{20} D/cm^2.

Fig. 7):

TDS spectra of the D_2 signal (a) of a-C, (b) of 2.5% and (c) of 7.5% a-C:W, which were exposed to a 200 eV D beam at 300 K and at different fluences (10^{17} D/cm^2, 10^{19} D/cm^2, 10^{20} D/cm^2).

Fig. 8):

Amount of retained D in 7.5% a-C:W, implanted to different temperatures between 300 K and 1300 K versus the fluence of incident 200 eV D. Specimens implanted above 300 K were pre-heated at 1300 K. Data points of pyrolytic graphite implanted at 300 K are shown for comparison.

Fig. 9):

Amount of retained D implanted at 900 K versus the fluence of incident 200 eV D. a-C and 7.5% a-C:W are compared to pyrolytic graphite. Specimens implanted at 900 K were pre-heated at 1300 K.

Fig. A1):)

Distribution of the local tilt angles of surface segments of 7.5% a-C:W, exposed to a 200 eV D beam between 300 K and 1100 K and at 10^{20} D/cm^2, measured by AFM over a scan area of 2x2 μm^2. If the FWHM is larger than $|12|^\circ$ and $|20|^\circ$ multiple surface crossings need to be taken into account in the NRA and the RBS spectrum, respectively.

figures

Fig. 1)

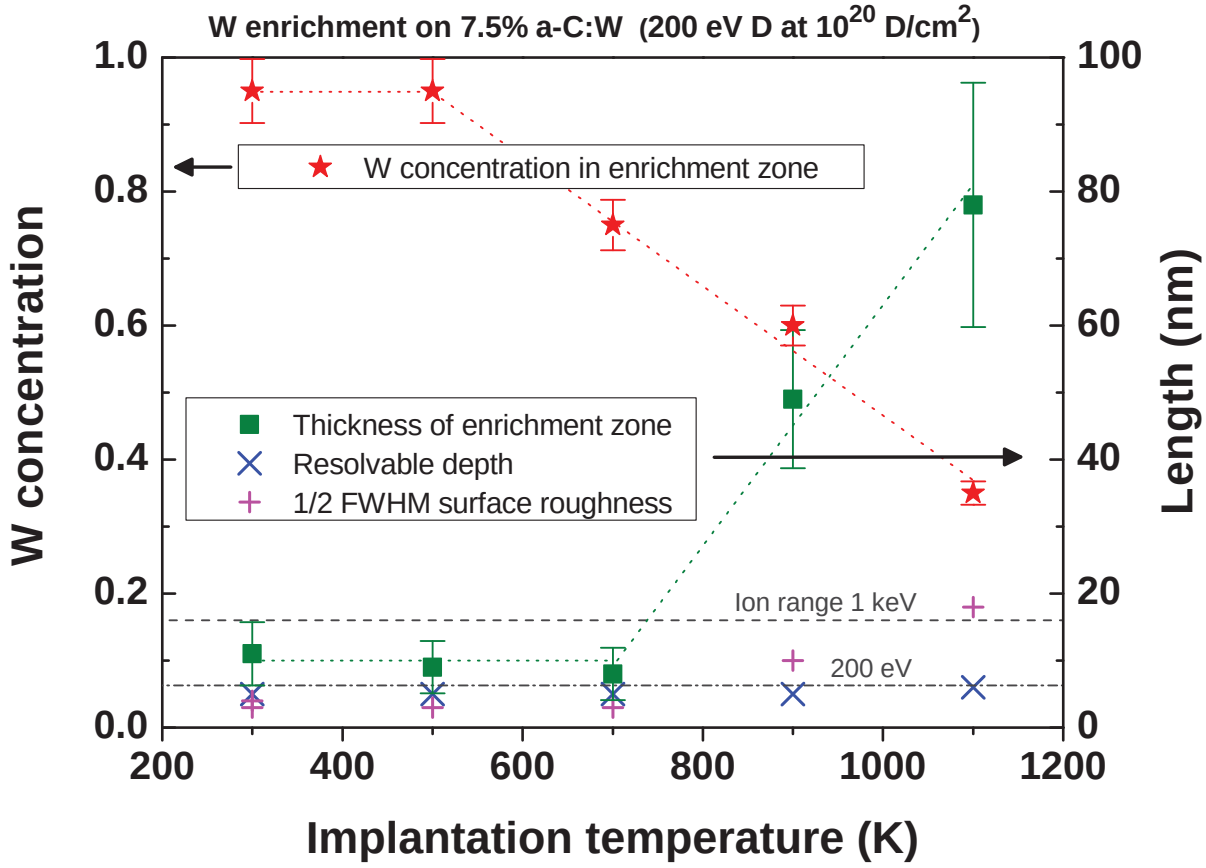

Fig. 2)

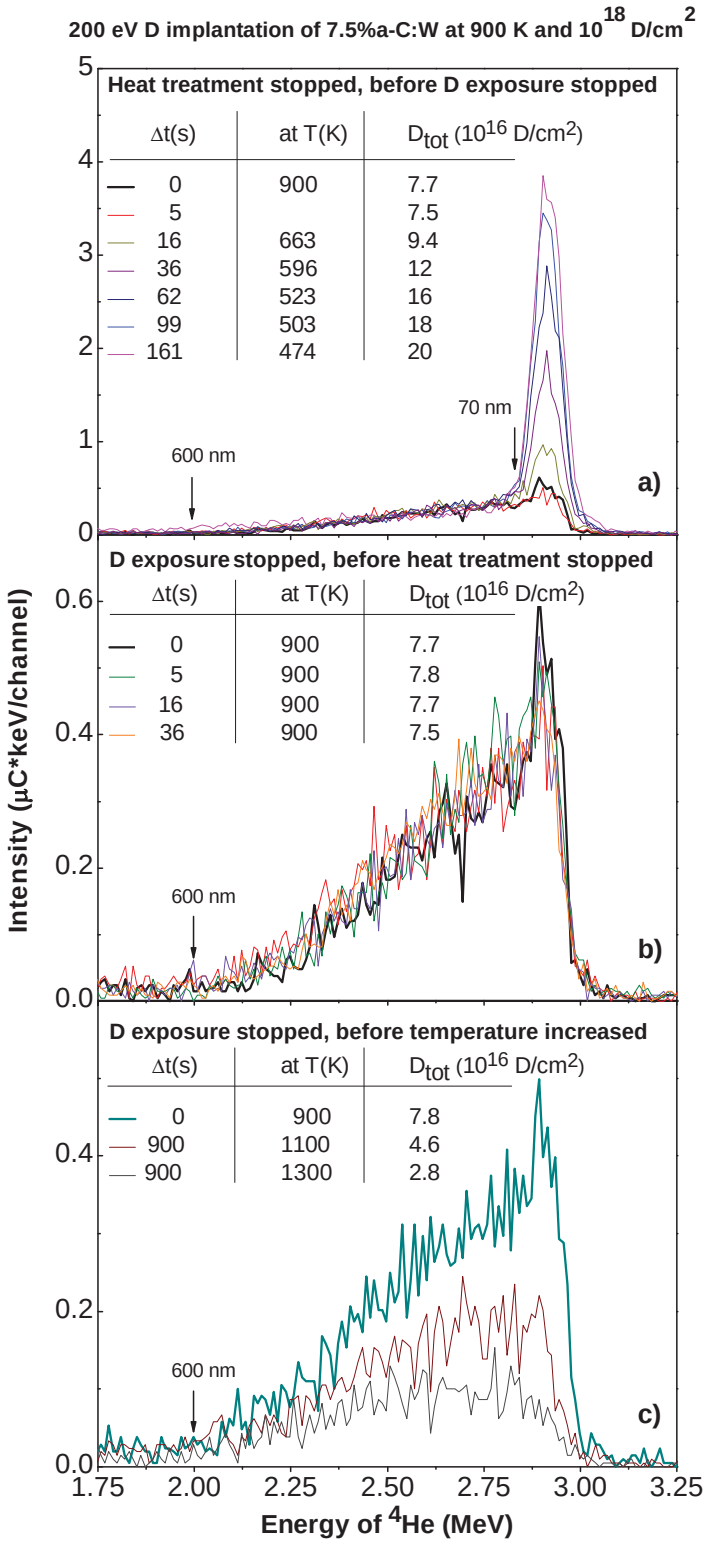
200 eV D implantation of 7.5%a-C:W at 900 K and 10^18 D/cm^2
Heat treatment stopped, before D exposure stopped
Δt(s) | at T(K) | D_tot (10^16 D/cm^2)
0 | 900 | 7.7
5 | | 7.5
16 | 663 | 9.4
36 | 596 | 12
62 | 523 | 16
99 | 503 | 18
161 | 474 | 20
70 nm
600 nm
a)
D exposure stopped, before heat treatment stopped
Δt(s) | at T(K) | D_tot (10^16 D/cm^2)
0 | 900 | 7.7
5 | 900 | 7.8
16 | 900 | 7.7
36 | 900 | 7.5
600 nm
b)
D exposure stopped, before temperature increased
Δt(s) | at T(K) | D_tot (10^16 D/cm^2)
0 | 900 | 7.8
900 | 1100 | 4.6
900 | 1300 | 2.8
600 nm
c)
Intensity (μC*keV/channel)
Energy of 4He (MeV)

Fig. 3)

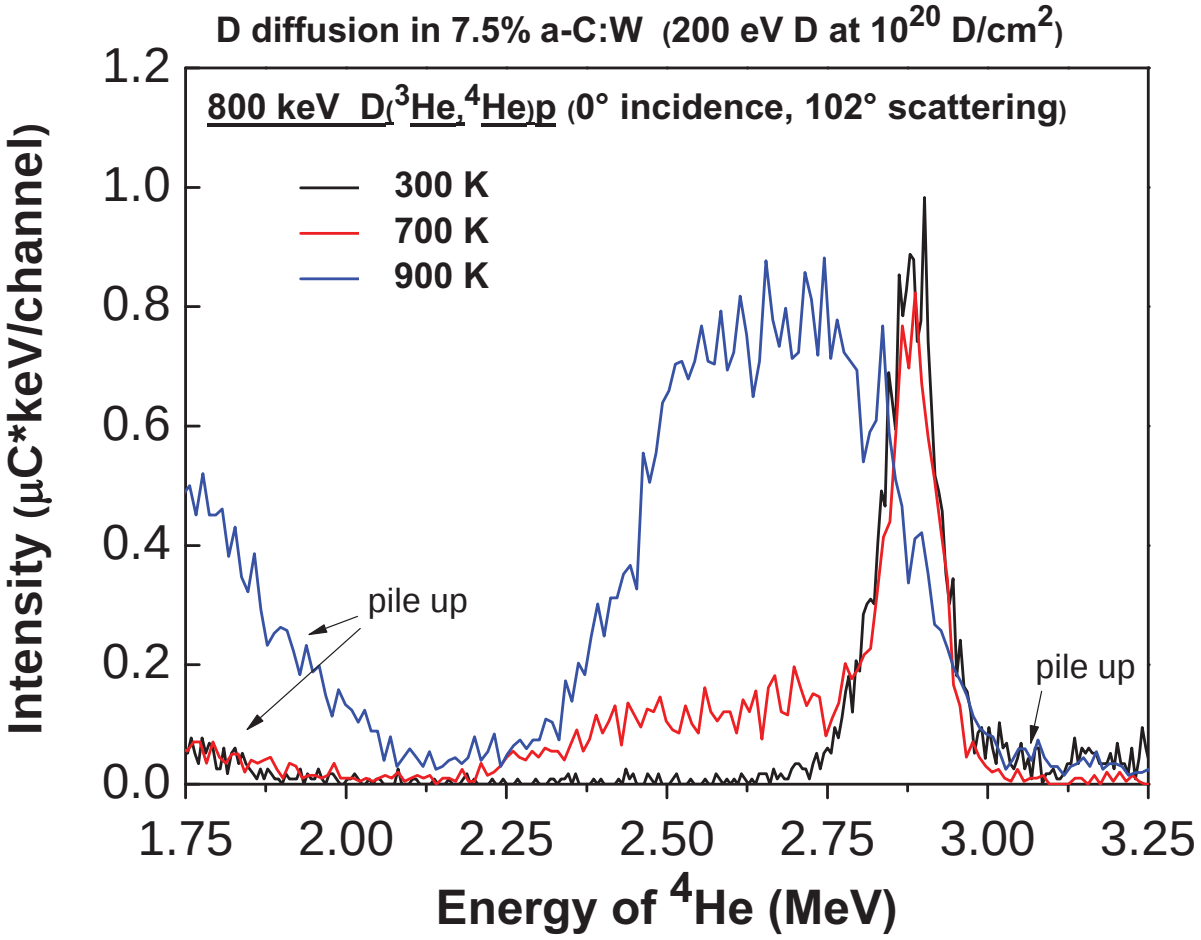
D diffusion in 7.5% a-C:W (200 eV D at 10^20 D/cm^2)
800 keV D(3He,4He)p (0° incidence, 102° scattering)
300 K
700 K
900 K
pile up
pile up
Intensity (μC*keV/channel)
Energy of 4He (MeV)
1.2
1.0
0.8
0.6
0.4
0.2
0.0
1.75
2.00
2.25
2.50
2.75
3.00
3.25

Fig. 4)

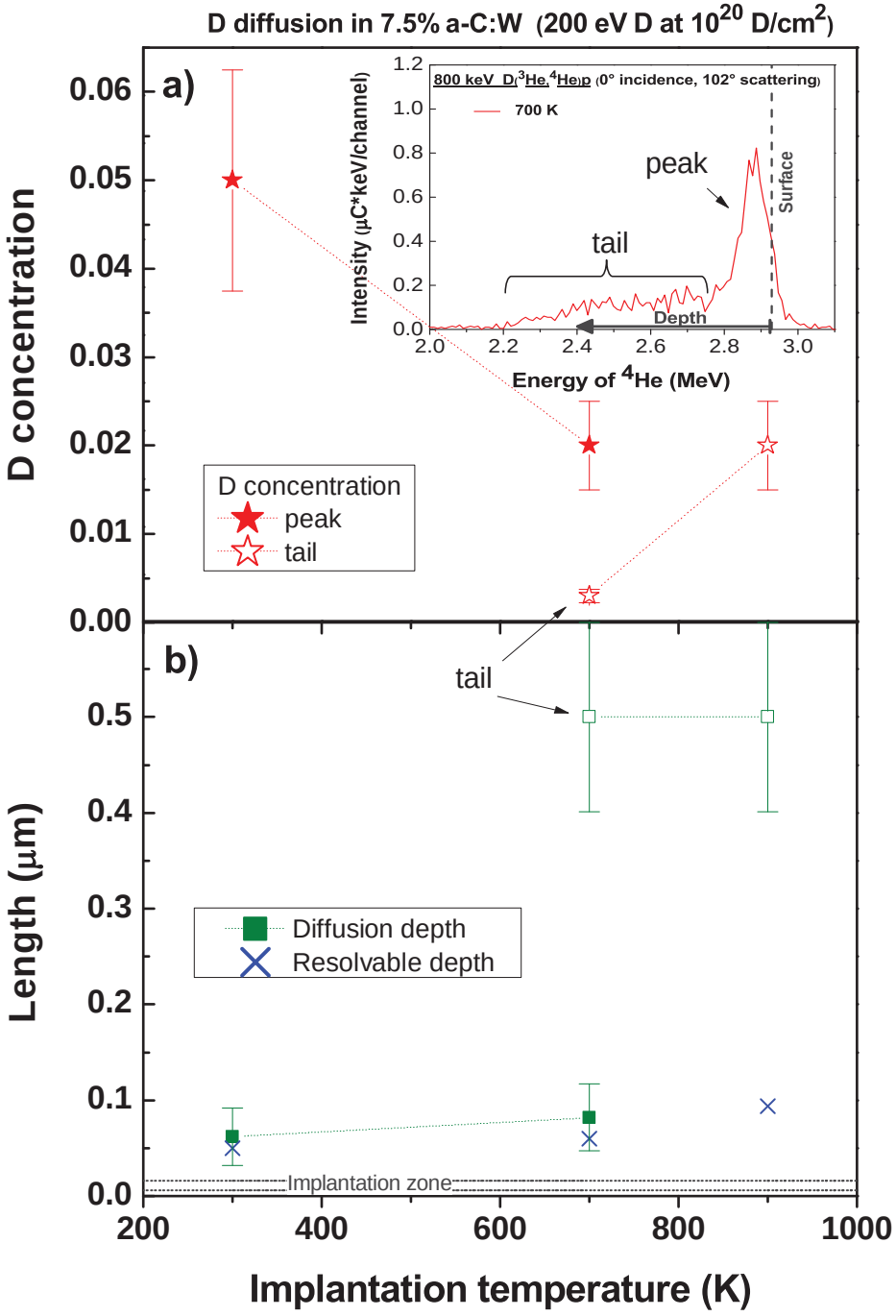
D diffusion in 7.5% a-C:W (200 eV D at 10^20 D/cm^2)
a)
b)
D concentration
peak
tail
800 keV D(3He,4He)p (0° incidence, 102° scattering)
700 K
Intensity (μC*keV/channel)
Energy of 4He (MeV)
Surface
Depth
Length (μm)
Diffusion depth
Resolvable depth
Implantation zone
Implantation temperature (K)

Fig. 5)

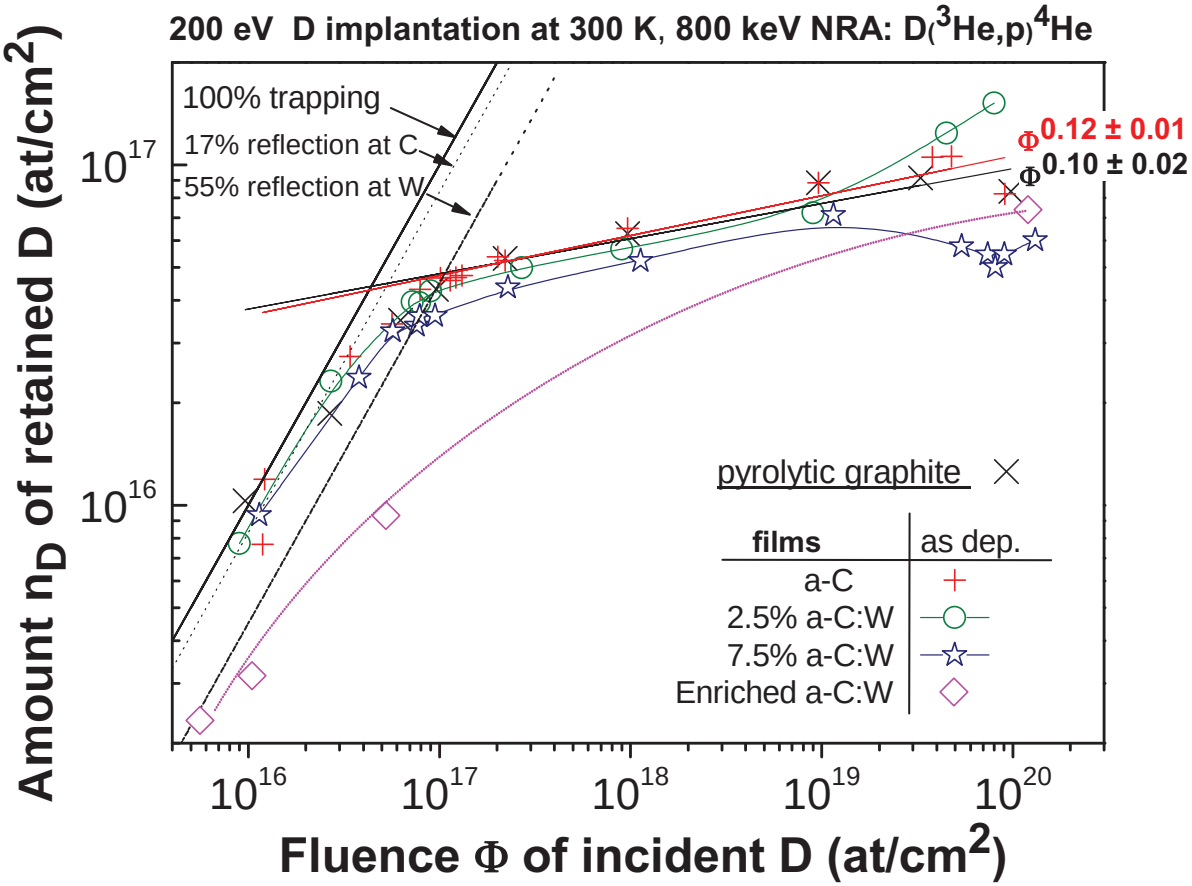
200 eV D implantation at 300 K, 800 keV NRA: D(3He,p)4He
100% trapping
17% reflection at C
55% reflection at W
Φ 0.12 ± 0.01
Φ 0.10 ± 0.02
pyrolytic graphite
films
as dep.
a-C
2.5% a-C:W
7.5% a-C:W
Enriched a-C:W
Amount nD of retained D (at/cm2)
Fluence Φ of incident D (at/cm2)
10^16
10^17
10^18
10^19
10^20

Fig. 6)

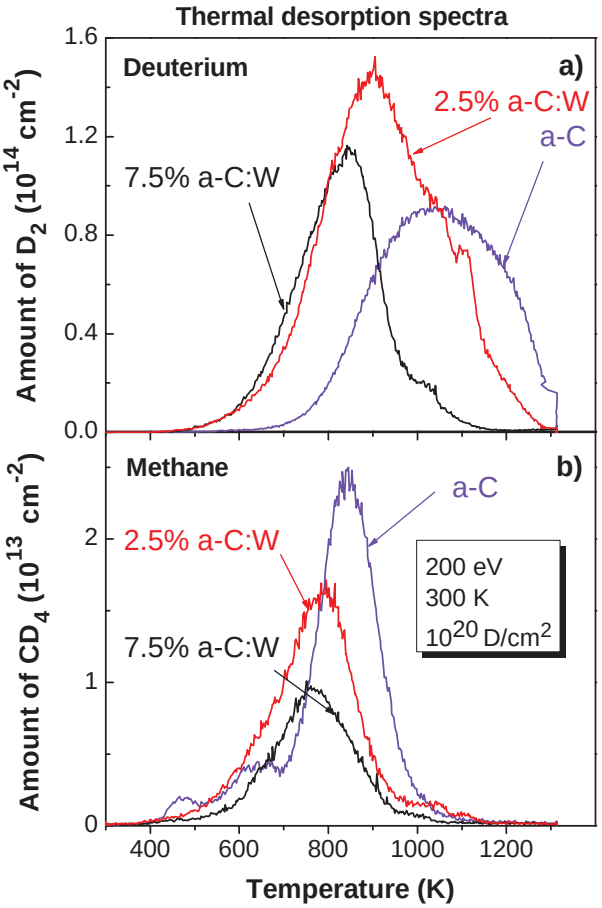
Thermal desorption spectra
Deuterium
a)
2.5% a-C:W
a-C
7.5% a-C:W
Amount of D2 (10^14 cm^-2)
1.6
1.2
0.8
0.4
0.0
Methane
b)
a-C
2.5% a-C:W
200 eV
300 K
10^20 D/cm^2
7.5% a-C:W
Amount of CD4 (10^13 cm^-2)
2
1
0
400
600
800
1000
1200
Temperature (K)

Fig. 7)

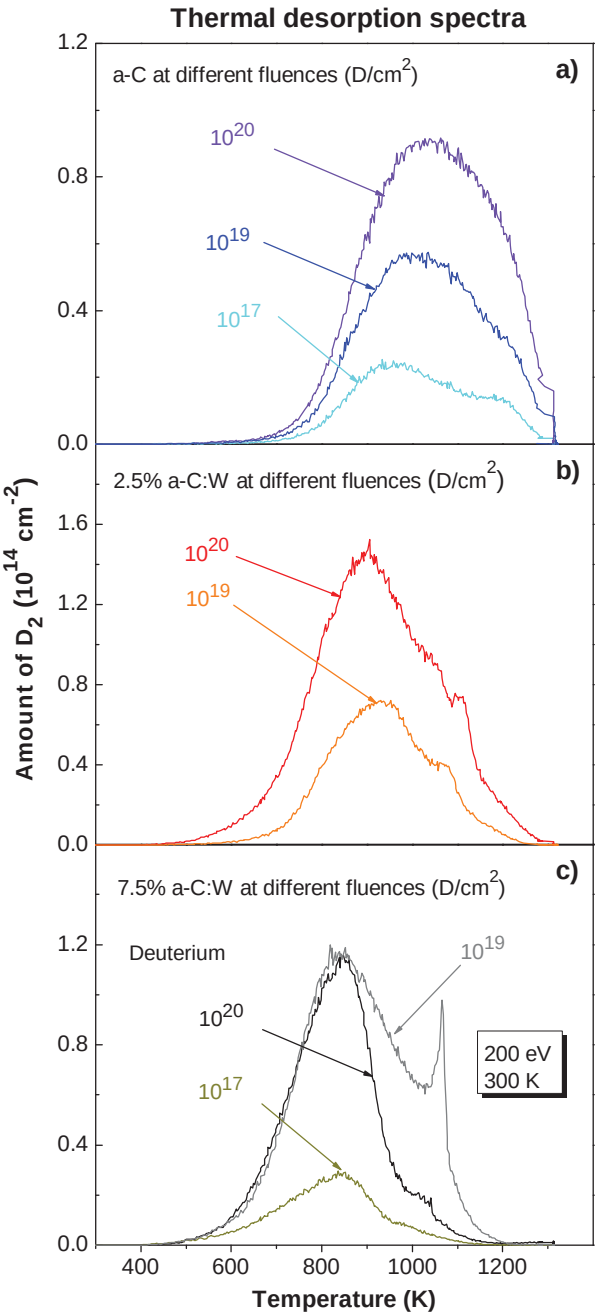
Thermal desorption spectra
a-C at different fluences (D/cm2)
a)
10^20
10^19
10^17
2.5% a-C:W at different fluences (D/cm2)
b)
10^20
10^19
7.5% a-C:W at different fluences (D/cm2)
c)
Deuterium
10^19
10^20
10^17
200 eV
300 K
Amount of D2 (10^14 cm^-2)
Temperature (K)
0.0
0.4
0.8
1.2
1.6
400
600
800
1000
1200

Fig. 8)

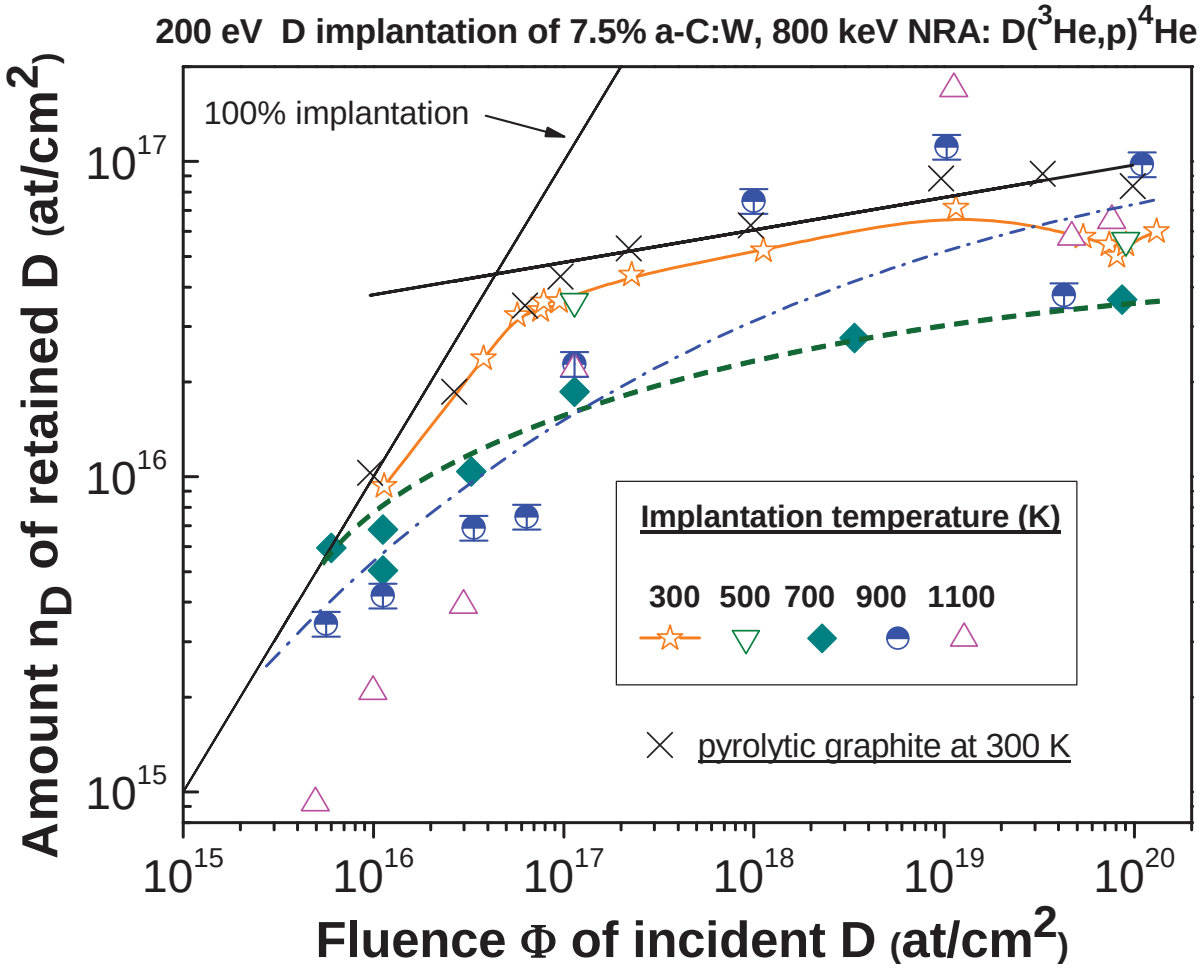
200 eV D implantation of 7.5% a-C:W, 800 keV NRA: D(3He,p)4He
100% implantation
Implantation temperature (K)
300 500 700 900 1100
pyrolytic graphite at 300 K
Amount nD of retained D (at/cm2)
Fluence Φ of incident D (at/cm2)
10^15
10^16
10^17
10^18
10^19
10^20

Fig. 9)

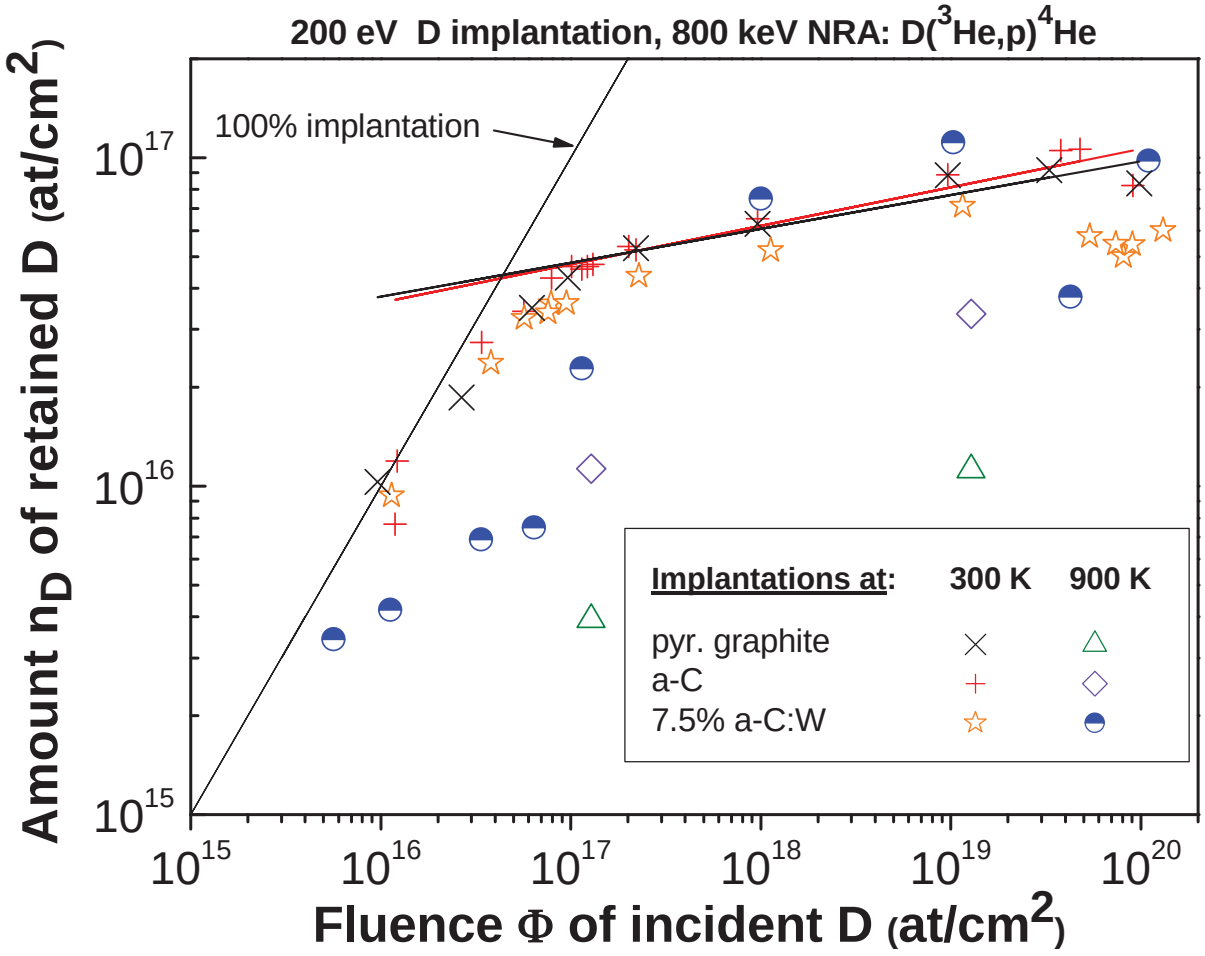
200 eV D implantation, 800 keV NRA: D(3He,p)4He
100% implantation
Amount nD of retained D (at/cm2)
Fluence Φ of incident D (at/cm2)
10^15
10^16
10^17
10^18
10^19
10^20
Implantations at: 300 K 900 K
pyr. graphite
a-C
7.5% a-C:W

Fig. A1)

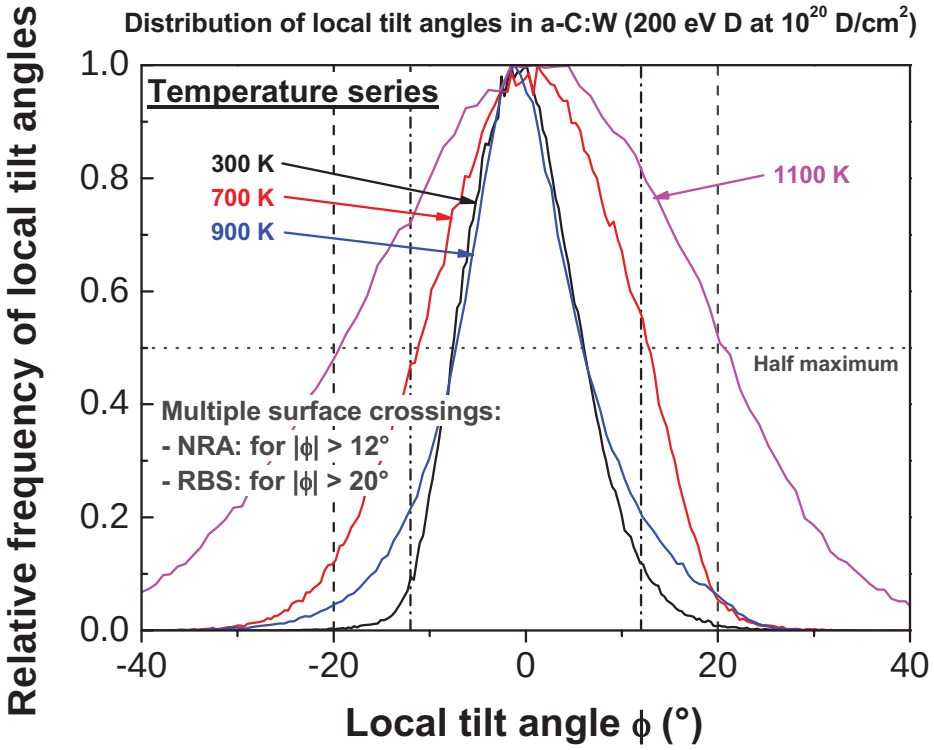
Distribution of local tilt angles in a-C:W (200 eV D at 10^20 D/cm^2)
Temperature series
300 K
700 K
900 K
1100 K
Half maximum
Multiple surface crossings:
- NRA: for |ϕ| > 12°
- RBS: for |ϕ| > 20°
Relative frequency of local tilt angles
Local tilt angle ϕ (°)
1.0
0.8
0.6
0.4
0.2
0.0
-40
-20
0
20
40